TECHNISCHE UNIVERSITÄT WIEN

D I P L O M A R B E I T

Development of a microfluidic nanotoxicological-screening system with integrated sensors for continuous monitoring of cell viability

Thema

Ausgeführt am Institut für

E163 Institut für Angewandte Synthesechemie
E164 Institut für Chemische Technologien und Analytik

der Technischen Universität Wien

Univ. Prof. Dipl.-Ing. Dr. Peter Ertl

unter der Anleitung von

durch

B.Sc. Reza Afkhami

Name

18. November 2019

Datum

Unterschrift (Student)

TECHNISCHE
UNIVERSITÄT
WIEN
Vienna University of Technology

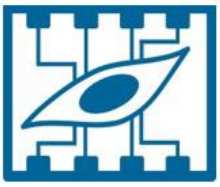

Cell Chip Group

Faculty of Technical Chemistry
Institute for Applied Synthetic Chemistry
Institute for Chemical Technologies and Analytics

Master Thesis

Development of a microfluidic nanotoxicological-screening system with integrated sensors for continuous monitoring of cell viability

Author Reza Afkhami

Supervisor Univ. Prof. Dipl.-Ing. Dr. Peter Ertl

November 2019 Vienna

Vienna University of technology

Faculty of technical chemistry

Institute of applied synthetic chemistry & institute for chemical technologies and analytics

Cell Chip Group

“Failure is an option here. If things are not failing, you are not innovating enough.”

– Elon Musk

Acknowledgments

Firstly I would like to express my sincere gratitude to my supervisor Prof. Dipl.Ing. Dr. Peter Ertl, for his continuous and generous support during my master thesis.

I would also like to thank Dr. Mario Rothbauer and Dr. Helene Zirath for their coaching, guidance, and insightful feedback on my work.

A big thank you also to all Cell Chip Group lab members for their patience in answering my newbie questions, sharing the sweets, especially the cookies, and for all the shared non-scientific casual conversations, particularly on nerdy topics.

Last but not least, I would like to thank my parents, my brother, my girlfriend, and my dear friends, especially the CORE, for their continuous encouragement and support.

Reza Afkhami

Contents

1 Abstract

With technological advancement and the emergence of nanotechnology, many unique nanoparticles are being developed. These particles offer a broad range of industrial, consumer, and medical applications. However, nanoparticles can enter the body via different means such as inhalation or dermal uptake, and when inside the body, they can circulate in the bloodstream and travel to the surrounding tissues or other organs such as placenta, which can impair the viability of the fetus or cause early childhood complications.

Nanoparticles have a different physicochemical characteristics compared to their bulk material, mainly due to their shape and size. Moreover, the high surface-to-volume ratio makes the nanoparticles extremely reactive, which potentially may result in oxidative stress, cytotoxicity, and genotoxicity. However, since the biological response to nanoparticles depends on their physicochemical properties, nanoparticles could interfere with some organic dyes used in cell-based assays, as well as with biological fluids such as cell culture medium. Therefore, the best approach to bypass limitations in nanotoxicity tests is to utilize at least two different *in vitro* toxicity or viability assays, as well as alternative screening methods such as microfluidics.

In this study, bewo b30 cells, derived from human placenta choriocarcinoma, are used to assess the toxicity effects of different nanoparticles via *in vitro* assays on the placenta model. PrestoBlue cell viability assay is used to investigate the toxicity of various nanoparticles in the presence of serum, as well as their time-dependent toxicity. Furthermore, Image-iT ROS detection kit has been used to evaluate oxidative stress caused by different nanoparticles at different concentrations and exposure times, with and without the presence of serum.

In this project, a microfluidic live-cell screening system with integrated optical oxygen sensors has been developed to analyze the nanotoxicity of different nanomaterials. Bewo b30 cells were cultured inside microfluidic chambers, representing a placenta model through which nanoparticles are passing or aggregated after exposure. Novel optical oxygen sensors have been integrated into the microfluidic chip. These sensors are label-free and non-invasive and enable fast and continuous monitoring of the cell-nanoparticle interaction during the entire exposure time. Different microfluidic protocols were established and optimized for both static and stop-flow measurements.

2 Introduction

2.1 Nanoparticles and nanotoxicity

Nanotechnology has received much attention in recent years, which led to the development of a wide range of nanoparticles with a variety of industrial, medical, and consumer applications. For example, titanium dioxide (TiO_2) and zinc oxide (ZnO) nanoparticles are broadly used in sunscreens and cosmetics to increase the ultraviolet (UV) light absorption and enhance sun protection factor [1]. Similarly, silicon dioxide (SiO_2) nanoparticles seemed to be very promising in the biomedical sector with a wide range of applications, including drug delivery, biomolecule detection and separation, and biomedical imaging [2]. Furthermore, various types of nanoparticles are used in the development of biosensors, such as silicon nanowire-based biosensors [3], [4], and semiconductor nanostructures like bioconjugated quantum dots [5]. Another application of nanoparticles in healthcare lies in the field of nanomedicine, which covers areas such as targeted drug delivery, nano diagnostics, and regenerative medicine [6].

Nanoparticles have a small size (at least one dimension ranging between 1 and 100 nm) [7], which leads to different physicochemical characteristics in comparison to their bulk material, including energy levels, optical properties, and chemical reactivity [8]–[10]. Although these properties lead to a wide range of applications in industry and healthcare, yet there can be potential health risks associated with these nanoparticles [6].

Shape and size are the main aspects of the difference in nanoparticle characteristics. High surface-to-volume ratio and the small size alone makes them highly reactive. Since the biological reaction to the nanoparticles varies depending on the size and shape, different toxicological methods are needed in comparison to the conventional toxicological assessment of soluble compounds, xenobiotics, or drugs. The toxicological tests carried on nanoparticles have to consider biodistribution and surface effects as well as the evaluation of the nanomaterial [6], [11]. Furthermore, there are many factors that cause mechanical-biological interactions between cells and nanoparticles. For example, nanoparticles that are stable and do not dissolve can accumulate in cells and provide a high surface-to-volume ratio, which eventually promotes surface-induced effects [12].

Nanoparticles could generate free radicals and reactive oxygen species (ROS) [13] from the molecules in their vicinity, due to increase in their reactivity and their high surface area, which may cause damage to cell membranes and proteins inside cells causing inflammation and oxidative stress [14], [15]. Nanomaterials can also split into ionic species when interacting with biological tissues or fluids such as gastric juice, which may lead to the release of reactive ions that could cause cytotoxicity [16], [17]. If nanoparticles disrupt DNA transcription and replication, genotoxicity may occur, which could remove genes from the sequence resulting in a range of harmful complications, such as apoptosis [18]–[20] or resulting in mutagenesis or carcinogenic outcome [21].

Because of the small size of nanoparticles and their high surface-to-volume ratio, nanoparticles actively interact with proteins and other cellular components. As soon as nanoparticles interact with biological fluids, bio-nano interface forms, which lead to the protein corona effect that impacts the biological responses to the nanoparticles, such as uptake, distribution, and toxic effects [12], [22]. Therefore, the properties of the nanoparticles can be significantly altered as soon as they interact with cell culture media containing serum. That means not only nanoparticle properties but also cell culture media composition can impact the cell-nanoparticle interactions [23].

Useful nanotoxicity assessments need to be high-throughput since the toxicity of nanoparticles is dependent on the particle composition, size, shape, and surface properties. Thus various nanomaterials should be analyzed. There are different cell and tissue types in the human body, and each can react differently to the nanoparticles, meaning that an optimal and stable nanotoxicology method should test a combination of human cells and nanoparticles [14].

2.2 Biological systems & Nanoparticles

Nanoparticles could enter the human body through ingestion, inhalation, or dermal uptake [24] or via direct injection in the case of nanomedicine [25], which may impair cell viability. Nanoparticles that are taken up inside the body can transit throughout the body via blood circulation and surrounding tissues and eventually might end up in organs such as kidney or spleen. Therefore, nanoparticles contact with cellular structures is inevitable, and they will most likely

penetrate the cells [26]. Figure 1 shows a diagram of tissues and organs that are accessible to nanoparticles after uptake via inhalation. The absorption of nanoparticles by different organs and tissues is dependent on the size of the nanoparticles. For instance, a study has shown that when polystyrene particles with different sizes ranging from 50 nm to 3 µm were ingested into a rat model, there was no evidence of particles above 100 nm in bone marrow and none larger than 300 nm were circulating in the bloodstream, while the 50 nm and 100 nm particles were absorbed in spleen, liver, blood, and bone marrow tissues [27].

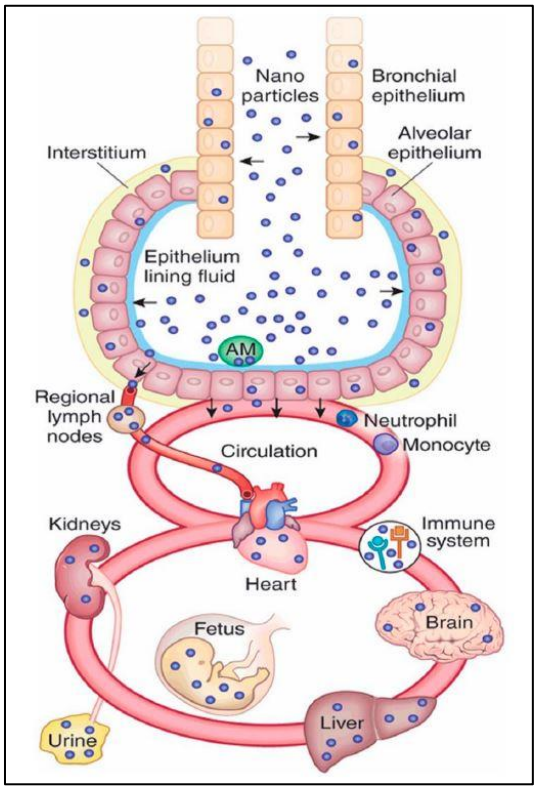

Figure 1. Diagram of nanoparticle pathway in the human body after inhalation [28].

Nanoparticles can penetrate the cellular membrane via passive transport mechanisms, such as diffusion and osmosis, which require no activation energy [29], [30]. Nanoparticles can also penetrate cells through active transport mechanisms when carrier proteins or ionic pumps within cell membrane attach to the nanoparticle and move them across the cell membrane into the cytoplasm with the use of energy [26]. Inorganic nanoparticles that require active transport to penetrate the cell membrane are usually stopped from entering cells, except for the particles that

are coated with a biomolecule such as transferrin (e.g., transferrin-conjugated gold nanoparticles) that promotes their absorption by the carrier proteins [31].

Nanoparticles that can not enter cells through membrane diffusion or membrane pores can penetrate the cell membrane via endocytosis [32]. Several studies have shown that nanoparticles are taken up based on size and shape by almost all cell types via endocytosis. Also, there are reports that nanoparticles have also been found in erythrocytes, which have lost their endocytosis abilities [26], [33], [34]. These results show that nanoparticles can passively penetrate cells, mainly through a mechanism that depends on the size and the shape of nanomaterials. Moreover, it is known that nanoparticles are sequestered significantly in the mononuclear phagocytic system [35], [36]. Particularly, uptake of nanomaterials by circulating monocyte-macrophages will eventually lead to their biodistribution in organs such as liver and spleen. For instance, some *in vivo* studies have shown that capturing of injected magnetic nanoparticles by macrophages leads to high levels of biodistribution in the liver and spleen [6], [37].

Some nanoparticles can change or bypass membrane permeability, based on their shape or their ionic potential. Nanoparticles that are pointy or have sharp edges can mechanically damage the cell membrane, creating short-lived nanochannels that provide a pathway for nanoparticles to enter the cytoplasm [38]. This mechanism can be useful in drug delivery, for example, by coating nanoparticles such as carbon nanotubes with biocompatible molecules that attach and penetrate cells or by creating nanoneedles that can mechanically penetrate cells and deliver drugs directly into the cytoplasm [14], [39].

The nanoparticle-cell interactions and pathways mentioned above are sophisticated and highly dependent on size and geometry, physicochemical properties, and surface characteristics of nanoparticles, meaning that high-throughput screening of nanoparticles on different cell and tissue types is significantly essential. In this study, the placental cell line Bewo b30 was chosen to perform an *in vitro* nanotoxicity, viability, and oxidative stress tests and to establish a lab-on-a-chip nanotoxicological system with integrated sensors to monitor the respiration and oxygen consumption of the cells.

2.2.1 The placental barrier model

The placenta is a temporary yet vital organ that develops during pregnancy and essential for maintaining the pregnancy [40], [41]. The most crucial function of the placenta is the exchange of endogenous and exogenous substances [42], which supplies the fetus with sufficient oxygen and nutrients, removal of fetal metabolic waste, and protection against harmful agents such as bacteria and viruses [43].

The placental transport takes place between the mother and the fetus via a multi-cellular complex consisting of villous syncytiotrophoblasts, villous cytotrophoblasts, and placental endothelial cells, which is often known as the placental barrier [44].

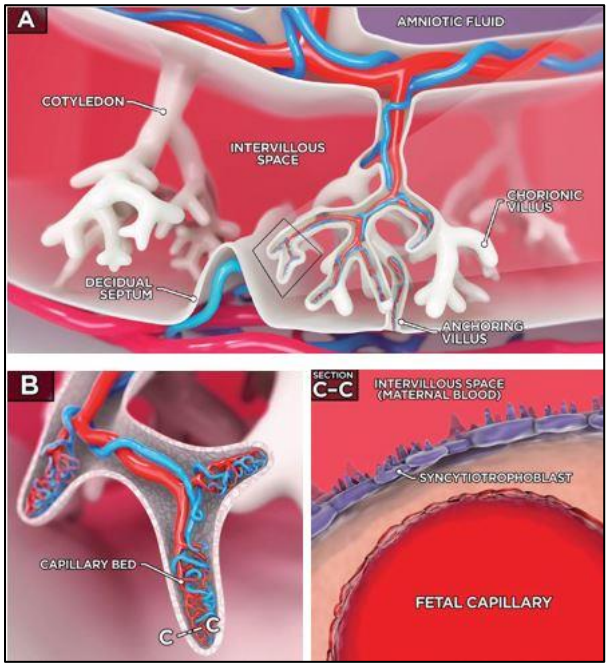

Figure 2. (A) Cross-section of the human placenta demonstrating, cotyledons that contain chorionic villi bathed in maternal blood. (B) A zoomed-in view illustrating the chorionic villi and inner fetal capillaries. (C) The placental barrier separates the maternal intervillous space from the fetal capillary lumen consists of syncytiotrophoblast and feta endothelial cells [45].

The mechanisms that are involved in the transport of substances through the placental barrier are mainly based on passive diffusion, facilitated diffusion, active transportation, and endocytosis/exocytosis [42], [43], [46], [47]. Furthermore, there are physiochemical factors which influence the placental transfer, such as umbilical cord blood flow, barrier thickness, concentration gradients, placental metabolism, and transporter activity in the placenta [48], [49].

Hypoxia (shortage of the oxygen supply) in the placenta threatens the vitality of the fetus as well as the viability of the placenta cells (cytotrophoblasts) [50]. Moreover, hypoxia, oxidative stress, and hypertension can cause pre-eclampsia, which affects 5% to 8% of women during pregnancy and is a critical factor in maternal and perinatal morbidity and mortality [51].

With the technological advancement and growing applications of nanomaterials, an increase in the nanoparticle production in the upcoming years is predictable. In recent years, researchers that are investigating the risks of nanoparticles are mainly focused on the cell and tissue types that may come in contact first with the airborne nanoparticles [52]. These airborne nanoparticles have raised concerns regarding the exposure risks during pregnancy and or early childhood [53]. It has now been shown that prenatal exposure to air pollution might be correlated to higher respiratory need and inflammation induction in newborns [54]. Furthermore, a recent study has provided compelling evidence of black carbon particles originating from ambient air pollution in the human placenta, which suggests direct exposure to the particles during the most vulnerable period of life [55].

These findings emphasize that nanoparticles could potentially penetrate the placental barrier and pose a threat to the fetus and have an impact on fetal and early childhood health. Therefore, the toxicity of nanoparticles and their risk assessment must be investigated thoroughly through conventional and novel nanotoxicology methods.

2.3 Conventional risk assessment of nanoparticles

Risk assessment of nanoparticles is more complicated compared to the traditional toxicology of chemical compounds [6]. Due to the vast and increasing number of available nanoparticles, there is an urgent need for nanotoxicology screening to investigate the immediate and long-term effects on human and environmental health.

Up until recent years, conventional approaches in toxicology assessments of nanoparticles were mainly *in vivo* animal testing. However, the most significant disadvantage of animal trials is the lack of correlation between findings in the *in vivo* models and the actual clinical effects due to the natural genetic differences between them, for instance, between rodents and humans [56], [57].

Moreover, often, improbable high dosages are applied to the models, which lead to acute toxicities, while the long-term effects of low concentration exposure remain unknown. Furthermore, animal trials are time and cost-intensive, which makes them inefficient to test a higher number of different nanoparticles [6].

To avoid some of the shortcomings mentioned above, *in vitro* cell-based assays are a more accessible and reliable alternative to the *in vivo* assessments of nanoparticle toxicity [58]. There are several advantages to *in vitro* toxicity assessments of chemical compounds and nanoparticles, including the reduction of animal testings, the speed, and lower costs compared to *in vivo* studies [59].

One of the many assays used in toxicity and cell viability tests are resazurin-based assays, such as alamarBlue and PrestoBlue assays, that quantify the metabolic activity of viable cells. Resazurin (7-hydroxy-3H-phenoxazin-3-one-10-oxide) is a nonfluorescent blue dye that in the presence of the redox environment of metabolically active and viable cells is reduced to resorufin, which is highly fluorescent pink dye [60]. Cells that are damaged or not viable are not capable of sustaining high reducing power, resulting in a relatively lower resorufin signal. Several studies have shown a favorable performance of resazurin-based assays in different cellular systems, such as HepaRG hepatic cell line [61], human epidermoid carcinoma cells (A431) [62] and a variety of melanoma cell lines [63].

Furthermore, studies have shown that various pathogenic particles [64] and nanoparticles [65], [66] produce reactive oxygen species (ROS) and free radicals. Therefore the evaluation of intracellular and extracellular ROS production is useful to assess the potential risk and toxicity of nanoparticles. Several methods with different sensitivity and specificity are available to evaluate the ROS production in the presence of cells, for example, assays based on the fluorescent dye 2,7-dichlorofluorescein (DCFH) can be used to measure ROS by flow-cytometric or fluorimetric techniques [59]. Another method involves luminescence assays that measure phagocytic burst based on chemical enhancers such as luminol or lucigenin [67], [68]. Moreover, electron paramagnetic resonance (EPR) can be used to measure cellular ROS by applying low-toxicity spin traps or spin probes such as TEMPOL (4-hydroxy-2,2,6,6-tetramethylpiperidine-1-oxyl) to the cell culture [59], for instance, the phagocytic burst of macrophages and neutrophils have been measured with EPR [69].

There are many other assays to measure *in vitro* toxicity and cell viability, such as lactate dehydrogenase (LDH) assay, trypan blue exclusion assay, propidium iodide (PI), luminescent adenosine triphosphate (ATP) detection assay and Live/Dead assay. However, it must be noted that nanoparticles could potentially interfere and behave differently in cell-based assays, for instance, carbonaceous nanomaterials have the potential to interfere in a variety of toxicity assays when assessed in human epidermal keratinocytes [59], [70]. Another disadvantage of *in vitro* nanotoxicity assessments is that engineered nanomaterials interact with organic dyes that are used in some cell-based assays, thus making them an unreliable option [71], [72]. Moreover, *in vitro* cell-based assays have poor control over the exposure of the cells to the nanoparticles, since their aggregation, sedimentation, and buoyancy can significantly change the number of nanoparticles that come in contact with cells, and therefore have an influence on the results [6]. Furthermore, it is often the case that *in vitro* cell-based assays are carried out under irrelevant physiological conditions since most nanotoxicity assessments use immortalized cell lines that are significantly different from native cells in human tissue [6], [73], [74].

Considering the limitations of the *in vitro* assays, the high number of engineered nanoparticles, different cells, and experimental requirements, the best approach to circumvent and tackle these issues is to use at least two different toxicity and/or viability assays, as well as employing innovative and robust techniques for nanotoxicology and nanomaterial risk assessment.

2.4 Microfluidics and risk assessment of nanomaterials

Microfluidic platforms are becoming an attractive alternative to the conventional *in vitro* toxicity and risk assessment assays. Microfluidic techniques have a variety of advantages over traditional technologies used in the assessment of nanoparticle-cell interactions (Figure 3). In particular, microfluidic devices allow recreating physiologically relevant measurement conditions, provide continuous monitoring, and maintaining stable suspension of nanoparticles during the measurement [6]. One of the most common objectives in microfluidics is to design and develop lab-on-a-chip devices that can perform analysis on a single chip [75], [76]. Lab-on-a-chip systems provide a wide range of applications such as cell-based drug testing and drug discovery [77],

microflow controlling and high precision fluid handling for high-throughput screening in the cell-based assays [78], and integration of sensors and detectors for *in situ* measurements and monitoring different parameters within the cell culture environment [75], [79].

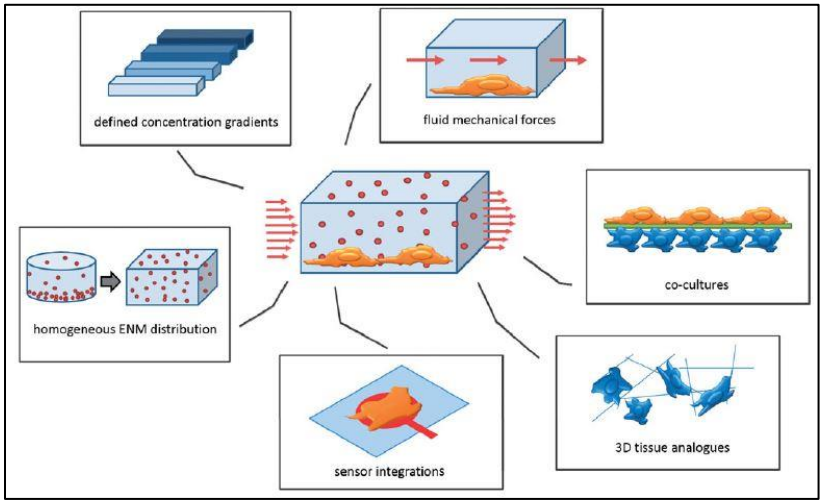

Figure 3. Advantages of microfluidics in risk assessment of engineered nanoparticles: microfluidic techniques can precisely control the nanoparticle concentrations and provide homogenous distribution of nanoparticles. Furthermore, integrated biosensors can be used in label-free and non-invasive monitoring of nanoparticle toxicity. Additionally, microfluidics is a suitable option to design and develop physiologically relevant *in vitro* test models by controlling fluid mechanics forces, co-cultivation of various cell types, and recreating 3D tissue models [6].

Although far from widespread, microfluidic nanotoxicity techniques are becoming popular among scientists, and new developments and advancements are being continuously published. There is a wide range of microfluidic methods and protocols for nanoparticle toxicity tests, and various devices have been developed, some of which are explained in the following section.

2.4.1 Microfluidic nanotoxicological systems

Microfluidics enables the possibility of introducing multiple biological conditions in a single system and replicates near *in vivo* like conditions and dimensions. Additionally, in the case of cellular analysis, microfluidic devices offer many advantages, such as small sample volume, controllability, and reproducibility. Thus, their benefits are promising in the development of high-throughput platforms for nanotoxicological screening applications. Small sample volume is a

crucial factor when dealing with nanotoxicology, since nanoparticles may be manufactured in low concentrations, and might be highly expensive, or there may be a limitation in the amount or dilutions which are required to perform toxicity tests. Furthermore, the performance of nanoparticles under the flow is more problematic to assess compared to macroscale particles. Therefore, the flow profiles and concentration gradients reproducibility rendered by microfluidic nanotoxicological systems is a significant advantage [14].

Mostly, nanoparticle toxicity tests are performed using well plates, meaning cells are exposed to the nanoparticles in static conditions, which may lead to absorbance or sedimentation of nanoparticles onto the surface of exposed cells under gravity. Often there is no adequate control over cell exposure to nanoparticles, resulting in aggregation and sedimentation of nanoparticles (Figure 4) [80].

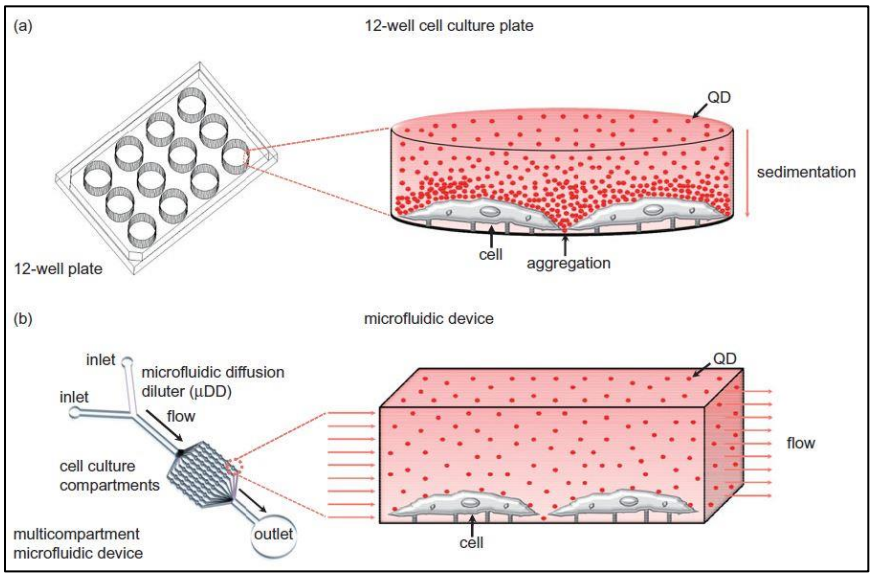

Figure 4. Diagram of nanoparticle kinetics in well plate vs. microfluidic device. (a) Nanoparticles (e.g., quantum dots) in static conditions (i.e., without flow in well plates) are sedimented due to gravity and tend to settle and aggregate. (b) The ability of the microfluidic device to keep a homogenous distribution of nanoparticles [80].

This issue has been investigated explicitly in a paper by Mahto et al. [80], in which they compared the static and flowing nanoparticles, by testing a sample of quantum dots in a cell culture well plate and then exposing the same quantum dot sample through a microfluidic concentration gradient generator device via cell culture medium to the cells. The static condition showed less cell viability and increased cell deformities suggesting the physiochemical stress caused by sedimentation of quantum dots on the cell membranes.

In order to study the effects of sheer-stress on the cells, the group of Kim et al. [81] has cultivated endothelial cells in a microfluidic chip and exposed them to the silica nanoparticles. Next, they adjusted the sheer-stress force to mimic the arterial and capillary shear-stress in a healthy human and compared the results to the static environment. The toxicity of particles has increased as shear-stress increased, while the static environment showed less toxicity at the same concentration. That means static nanotoxicity assays may not be the best option to represent the actual toxicity in a human body.

Furthermore, single-cell microarrays can be used to trap and immobilize cells, which allows for specific evaluation toxicity and viability tests on individual cells apart from their population as in typical cell toxicity and viability assays. A microfluidic single-cell device based on polydimethylsiloxane (PDMS) has been developed by Cunha-Matos et al. [82]. They trapped primary bone marrow dendritic cells in single-cell pockets within the microfluidic chamber formed by soft lithography and then introduced gold nanorods to the traps. They monitored the cells for 24 h in a live-cell incubator and evaluated individual trapped cells for their response to the gold nanorods.

As an example of integrated sensors, the group of Rothbauer et al. [83] has developed a microfluidic cell culture device with integrated impedance sensors for non-invasive and continuous monitoring of cells under dynamic exposure of silica nanoparticles. Human lung adenocarcinoma cells were seeded in the microfluidic chip in media containing serum to form a confluent monolayer of cells over the electrode surface. Nanoparticles perfusion carried out under flow and with a serum-free media (to prevent bioactivity of the nanoparticles). Once again, full media containing serum was perfused, to enable the regeneration of the cells. Additionally, a metabolic assay was carried out in parallel to impedance measurement, which showed that silica nanoparticles had reduced the cell regeneration and surface re-attachment. Moreover, the microfluidic flow within the device reduced the regenerative capacity of the cells, meaning that shear-stress applied to the cells influences the nanoparticle uptake increase and toxicity.

2.4.2 Oxygen biosensors

Oxygen plays an essential role in mammalian cell culture. The consumption of oxygen is a crucial and useful signal for understanding the behavior of cells, their functionality, and the assessment of their viability. Oxygen concentration varies hugely in the human body, from 0.5% in tissues such as cartilage and bone marrow and up to 14% in the lungs and circulatory system [84]. Despite this variation in oxygen demand throughout the human body, most in vitro cell culture are preformed under ambient atmospheric oxygen, which is an elevated level equivalent to 21% oxygen. This condition is referred to as hyperoxia and could impact cell behavior [85]. Insufficient oxygen levels, or hypoxia, has a profound effect on cells and tissues such as inducing vasodilation [86] and shifting metabolic process to reduce oxygen consumption [79].

Oxygen level is an essential parameter in stem cell cultivation and differentiation. Oxygen level changes in the stem cell cultivation environment can be used to establish an *in vitro* disease model [87]. The interest in controlling and monitoring the oxygen levels in mammalian cell culture has led to the utilization of a wide range of sensing methods such as standard electrochemical electrodes [88], enzymatic sensors [89] and fluorescent and luminescent optical biosensors [90].

Optical sensors based on oxygen-sensitive dyes which are embedded in a polymer matrix are a suitable option for integration in a lab-on-a-chip device due to the effortless integration of the sensor spots in the microfluidic channels, their reliability, cost efficiency, and their long term stability [91]–[94]. The surrounding oxygen molecules alter the luminescent intensity and decay time of the phosphorescent indicator dye, which provides information on oxygen concentrations [95]. Among these types of oxygen sensors, porphyrin-based sensor dyes are highly suitable due to their biocompatibility and sensitivity [96], [97]. A typical microfluidic oxygen monitoring systems consist of the biochip, optical fiber, a read-out system, and a data acquisition device [95], [98]. For example, in a recent paper by Zirath et al. [94], oxygen indicator sensors based on platinum (II) meso-tetra (4-fluorophenyl) tetrabenzoporphyrin (PtTPTBPF) were integrated into two different microfluidic chips (Figure 5) to monitor dissolved oxygen levels and cellular oxygen respiration in 2D and 3D microfluidic cell culture environment. The monitoring of partial oxygen pressures provided the estimation of respiration in cell monolayers under the influence of microfluidic flow, different cell types, cell numbers, and extracellular matrix (ECM) coatings.

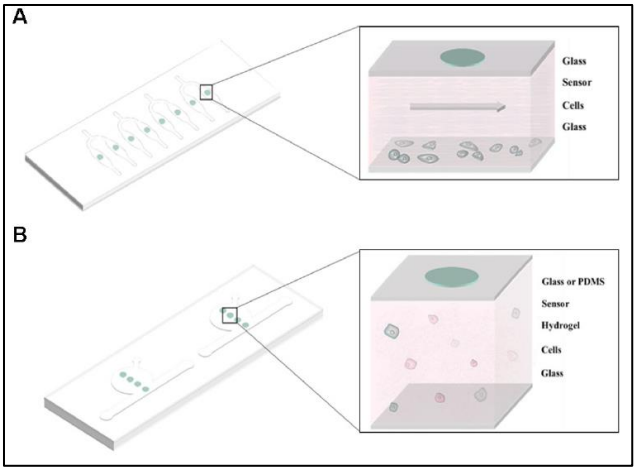

Figure 5. Schematic model of, (A) 2D culture chip and, (B) 3D culture chip with integrated PtTPTBPF oxygen sensors[94].

The integrated oxygen sensors mentioned above are non-invasive and label-free, which enables the continuous and real-time monitoring of oxygen levels, metabolic activity, oxygen consumption rates, and cell viability [94]. Therefore, in this study, a similar microfluidic device with PtTPTBPF integrated oxygen sensors has been developed, and a microfluidic system has been optimized to investigate the toxicity of nanoparticles on bewo b30 cells and monitor their oxygen consumption and viability.

3 Materials and Method

3.1 Cell culture

For this study BeWo b30 cells (generously provided by Dr. Tina Bürki-Thurnherr, EMPA, Switzerland) were cultured in Dulbecco's Modified Eagle's Medium (DMEM with L-glutamine and high glucose; Gibco, 11965-084) and Ham's Nutrient Mixture F12 , 10 % Fetal Calf Serum (FCS, PAA, A15-101), 1% Antibiotics (Gibco, 15240-062) and 0.5 % HEPES (Sigma Aldrich) at 37º C with 5% CO2.

Cellstar filtered screw cap culture flasks (Item No.658175,250 ml,75 cm^2,PS,TC,sterile) were used to culture cells. Cells were washed twice using Phosphate Buffered Saline (PBS), and 2ml of

trypsin (Sigma-Aldrich Trypsin-EDTA solution) was added into the flask to dissociate adherent cells following with 3-5 minutes of incubation, 5 ml of complete media was added to stop the trypsinization, and the suspension was moved into an empty falcon tube. Cells were centrifuged for 5 minutes with 140 rcf, and after centrifugation, the supernatant was removed, and 6 ml of complete media was added to dilute the cell pellet for cell counting.

Cells were seeded with 50k cells/cm^2 per well in a 38 well plate for presto blue and ROS assays and 400 k/ml were used for seeding the cells in the chip for oxygen consumption measurements.

3.2 Nanoparticles

For nanotoxicology and nanoparticle screening, various nanoparticles have been used, which are Silicon Dioxide ICN (HISENTS project), and nanoparticles obtained from the European commission's joint research center (JRC), including Silicon Dioxide, Titanium Dioxide, and Zinc Oxide.

Nanoparticle	Solvent	Concentration	TEM d(nm)	DLS (Intensity) d(nm)	DLS (Number) d(nm)
SiO_2 ICN (HISENTS)	Mili-Q water	10.15 mg/mL	34.9 ± 4.15 nm	77.3 ± 35.9 nm	36.7 ± 2.61 nm
SiO_2 JRC (NM02000a)	Mili-Q water	10 mg/mL	Sample present aggregation	3178 ± 340.3 nm	3131 ± 340.3 nm
TiO_2 JRC (NM01001a)	Mili-Q water	20 mg/mL	Sample present aggregation	789.7 ± 29.7 nm	684.2 ± 35.83 nm
ZnO JRC (NM62101a)	Mili-Q water	20 mg/mL	Sample present aggregation	Peak1 146.0 ± 15.0 nm Peak2 1626 ± 299.4 nm	Peak1 140.9 ± 21.2 nm Peak2 1536 ± 324 nm

Table 1. Nanoparticle specification provided by Inorganic Nanoparticles Group (Catalan Institute of Nanoscience and Nanotechnology)

To prepare a serial dilution, nanoparticles must be resuspended in an ultra-sonic bath for 5 minutes, and the required volume of nanoparticles to obtain a concentration of 500µg/ml must be calculated.

For this study, 1:2 serial dilution to obtain six concentration of nanoparticles plus a negative control (only media) has been used. (see Table 2 as an example of dilution process for SiO_2 ICN)

	Concentration	Dilution	Final volume:
S	10.15 mg/mL	Stock solution	
NP1	500 µg/mL	148 µL of **S** + 2824 µL of medium	1500 µL
NP2	250 µg/mL	1500 µL of **NP1** + 1500 µL of medium	1500 µL
NP3	125 µg/mL	1500 µL of **NP2** + 1500 µL of medium	1500 µL
NP4	62.5 µg/mL	1500 µL of **NP3** + 1500 µL of medium	1500 µL
NP5	31.25 µg/mL	1500 µL of **NP4** + 1500 µL of medium	1500 µL
NP6	15.625 µg/mL	1500 µL of **NP5** + 1500 µL of medium	3000 µL
NP7	0	Only medium	

Table 2. Serial dilution of SiO2 ICN (10.15 mg/mL, HISENT project)

3.3 PrestoBlue™ cell viability assay

To evaluate cell viability and nanotoxicity screening of nanoparticles, PrestoBlue™ cell viability reagent (LOT 1922837, Thermo Fischer Scientific) has been used. Cells were cultured in the 48 well cell culture plate (LOT E17113LN, CELLSTAR ®, Greiner bio-one).

To achieve a confluent monolayer of cells, well plates (21 wells, Triplicates of each nanoparticles concentration) were seeded with 50k cells/cm^2. After 24 hours incubation time, well plates were washed with phosphate-buffered saline (PBS), and media were changed to the desired media and nanoparticles combination. (e.g. 500µg/ml with 10% serum). To assess the toxicity of nanoparticles, we exposed the cell for 4 and 24 hours.

PrestoBlue solution was prepared shortly before finishing of the incubation (4h and 24h). 10% of PrestoBlue in complete medium were prepared in darkness and covered by aluminum foil. After removing the nanoparticle solution and washing the wells with PBS,300µl of PrestoBlue solution was added in each well, and the well plates were covered by aluminum foil following with 30-60 minutes of incubation. Afterward, 100µl was removed from each well of 48 well plates and added to 96 well F-Bottom microplates (LOT E18083TQ, chimney well, white, lumitrac, Greiner bio-one), and additionally, prestoBlue solution was added in three empty wells as a blank control.

To perform the fluorescence intensity measurement, PerkinElmer multimode EnSpire 2300 plate reader was used. Top excitation filter was used to perform this experiment, and excitation

and emission wavelength were 560nm and 590nm, respectively. Moreover, Measurement height was adjusted via plate reader settings to increase the measurement accuracy.

3.4 Image-iT™ LIVE Green Reactive Oxygen Species Detection kit

For ROS detection in live cells exposed to nanoparticles, The Image-iT™ LIVE Green Reactive Oxygen Species (ROS) Detection Kit (I36007, Invitrogen detection technologies, Thermo Fischer scientific) was used. The assay is based on 5-(and-6)- carboxy-2′,7′-dichlorodihydrofluorescein diacetate (Carboxy-H_2DCFDA), and additionally the tert-butyl hydroperoxide (TBHP) is provided by the kit as a positive control for ROS induction. It is recommended to use Hank's balanced salt solution with calcium and magnesium (HBSS/Ca/Mg, Gibco, 14025-092).

Cells were cultured in the 48 well cell culture plate (LOT E17113LN, CELLSTAR ®, Greiner bio-one) as duplicates for each concentration plus the ROS positive control compound(TBHP), with 50k cells/cm^2 seeding density for 24 hours before nanoparticle exposure to achieve a confluent monolayer of cells. After the incubation, cells were washed with PBS and exposed to nanoparticles with the concentrations mentioned in table 2 (section 4.2) for 4 hours and 24 hours. Besides, extra wells were seeded for inducing the cells later with ROS positive control compound (TBHP). 100mM stock solution of TBHP was prepared by adding 1.0µL of TBHP (Provided by kit, Component C, 7.78 M) to 77µL of sterile distilled water. The 100mM TBHP stock solution was diluted 1:1000 in the complete media to prepare a 100µM TBHP working solution. A sufficient amount of the 100µM TBHP working solution was applied to the cells during the last hour (60-90 minutes) of the nanoparticles incubation period at 37°C and 5% CO_2.

To label the cells with carboxy-H_2DCFDA, first, a 10mM stock solution must be prepared. To prepare the stock solution 50µl of DMSO (Provided by kit, component D) must be added to one vail of carboxy-H_2DCFDA (Component A, 275µg) and vortexed the vial the powder is completely dissolved. Next, 15µl of the 10mM carboxy-H_2DCFDA stock solution was added to 6 (5µL per 2mL) ml of warm HBSS/Ca/Mg to prepare a 25µM carboxy-H_2DCFDA working solution. Exposed cells were washed with warm HBSS/Ca/Mg once and labeled by adding 185µl of the 25µM carboxy-H_2DCFDA to each well. Culture plates were covered by aluminum foil to protect against light and incubated for 30 minutes at 37°C and 5% CO_2. Next, cells were washed carefully

three times with HBSS/Ca/Mg and mounted in a warm buffer. Imaging must take place immediately for the best results. The excitation/emission maxima of the oxidation product are approximately 495/529, and the standard fluorescein filter sets can be used for imaging the well plates. Furthermore, background noise was eliminated using Fiji, which is an open-source image processing software based on ImageJ.

3.5 Microfluidic chip with integrated oxygen sensors

An oxygen-tight microfluidic chip has been developed to measure the dissolved oxygen in microfluidic chambers. The chip is made of two microscope slides (VWR Microscope Slides, Ground Edges, article No. 631-1552), two layers of ARcare® 8259 which is a white rigid plastic film and is coated one side with a medical-grade pressure-sensitive adhesive and has a thickness of 157.48 µm without liners, and one layer of ARcare® 90445, which is a transparent plastic film with a medical-grade pressure-sensitive adhesive on both sides and the thickness of 81.28 µm.

Inlet holes were drilled to prepare the microscope slides for bounding, and sensor spots were roughened using the drill, and together with the bottom slide, they were washed in the ultrasonic bath for 5 minutes using 2% Hellmanex solution and rinsed three times afterward with DI water. After drying the slides, the PtTPTBPF oxygen sensor was applied by pipetting (2-3µl per spot) on the top slide. Since the oxygen sensors are covalently bonded to the glass, the rough surface improves their bounding. Sensors were dried and bounded to the glass at room temperature for 2 hours.

The microfluidic pattern was developed with micro-cutting the CAD design on ARcare® 90445 and ARcare® 8259 films using Roland CAMM-1 GS-24 vinyl cutter. Two layers of ARcare® 8259 were prepared and bonded on top of each other and then bounded carefully to the bottom microscope slide. To bond, the top glass slide with integrated oxygen sensors to the bottom slide, which is bonded to two layers of ARcare® 8259, double-sided transparent ARcare® 90445 film was micro-patterned using the Roland vinyl cutter. The total height of the microfluidic chamber is approximately 400 µm, and the volume of the chamber is roughly 10 µL. The last step of chip development is to glue the inlet tubing to the microfluidic chip using Tygon tubing and epoxy glue.

3.6 Microfluidic setup with optical oxygen meter - FireSting

The chip was mounted on a 3D printed platform with a fiber holder and placed in a heating chamber. The syringe pump was used to pump the media into the chambers, and in order to control the flow and eliminate the air bubbles, 4-way flow valves were employed. Falcon tubes were used to store the outflow waste from microfluidic chambers and 4-way flow valves. FireStingO_2 optical oxygen meter (Pyroscience, Germany) was used to monitor the oxygen consumption Optical fiber with the length of 1 m, the outer diameter of 2.2 mm and fiber diameter of 1 mm was connected to the FireStingO_2 and mounted on the chip, and factory calibration conditions were used to calibrate the sensors.

Cell respiration was measured on-chip under both static and flow conditions. For the static oxygen monitoring, cells were seeded in the chip and mounted on the microfluidic platform, and oxygen consumption was monitored continuously for hours. In the case of flow measurements, an optimized protocol was used to record three cycles of stop-flow. The cycles consist of 10 minutes of flow with 10 µL and 5 minutes of stop-flow to monitor oxygen consumption. Stop comments were entered in the O_2 logger application (e.g., stop1, lower case, and no space) to find the data sets from the raw data file.

3.7 Single-cell microarray fabrication

The single-cell microarray is a PDMS based microchip, developed by the soft lithography technique. PDMS is mixed in a ratio of 10:1 with the curing agent provided by the kit, to prepare the PDMS for baking and thus hardening. Next, the mixture is poured on a silicon-based mold, containing the structure of the microarray, and then place in a vacuum chamber to eliminate the bubbles. Then the wafer and bubble-free PDMS mixture are baked in the oven for 1 hour at 70°C. The next step is to remove the PDMS layers from the wafer and place them in a clean Petri dish with structure facing upwards to avoid damaging and contamination of the channels.

Microscope slides (VWR Microscope Slides, Ground Edges, article No. 631-1552) were used as the bottom layer of the chip. The microscope slides were washed in the ultrasonic bath for 5 minutes using 2% Hellmanex solution and rinsed three times afterward with DI water. The next step is bonding the PDMS layers, and microscope slides using the plasma cleaner. After activating the surface for bonding, the PDMS must be gently pressed on the microscope slide to avoid damaging the microstructure of the array. The bonded chips were clamped and placed in the oven for 1 hour at 70°C. The last step is sterilizing the microchips using 70% ethanol and washing them with sterile PBS. Bewo b30 cells were diluted to 10 k/ml and seeded carefully with a syringe.

4 Results and discussion

4.1 Toxicity assessment using PrestoBlue™ cell viability assay

The toxicity of various nanoparticles was evaluated using PrestoBlue™ cell viability assay. Bewo b30 cells were cultured in a 48 well plate with 50k cells/cm^2 seeding density and incubated for one day to form a confluent monolayer of cells. In this assay, nanoparticles were diluted in different concentrations (Table 2), plus a negative control being only the cells with cell culture media. Cells were exposed to three different nanoparticles (SiO_2 ICN, SiO_2 JRC, and ZnO JRC) for 4 and 24 hours to investigate the concentration, exposure time, and time-dependent effects of different nanoparticles on the cells. Another aspect was the evaluation of the serum in the cell culture media. Hence cells were cultured with 10% FCS and 0% to investigate serum starvation and its consequences on the sells and to assess the toxicity of nanoparticles in the absence or the presence of the serum.

The cell viability was calculated by the following equation, and results were grouped and plotted using GraphPad Prism 6 (Figure 5)

$$Cell\ Viability\ (\%) = 100 \times \frac{RFU_{ConcentrationX} - RFU_{Blank}}{RFU_{Control} - RFU_{Blank}}$$

The results show that SiO_2 ICN (Figure 5A, B) nanoparticles have no toxic effect at the most concentrations in the presence of serum (10% FCS). There is a slight reduction in cell viability in

500 µg/ml concentration at 4h exposure (Figure 5A), and a lesser cell viability reduction in 125 µg/ml and 250 µg/ml at 24h exposure (Figure. 5B). However, 500 µg/ml concentration at 24h shows cell viability around 50% of the control (Figure. 5B). In the case of serum starvation, there is a significant loss of cell viability at 250 µg/ml and 500 µg/ml concentrations under 4h exposure (Figure 5A) and an evident decrease in cell viability at 24h exposure (Figure 5B).

Interestingly, SiO_2 JRC appears to induce more toxicity compared to SiO_2 ICN. As demonstrated in figure 3C and figure 3D, there is a decrease in the cell viability at both 4h and 24h exposure, particularly at 250 µg/ml and 500 µg/ml concentrations. However, in the case of 0% FCS, there is a significant decrease in the viability at all concentrations at both 4h and 24 exposure.

Silicon dioxide (SiO_2) nanoparticles have various industrial or consumer applications such as additives to cosmetics, drugs, printer toners, paper, tires, varnishes, and food as well as biomedical and biotechnology applications. Some *in vitro* studies have shown size- and dose-dependent toxicity, increased ROS levels, production of inflammatory mediators, and cellular uptake of SiO_2 nanoparticles [99], [100]. However, the adverse effects of SiO_2 nanoparticles were significantly less in the presence of serum (10% FCS), likely due to the masking of reactive surface groups [100].

The most remarkable result is the significant toxicity of ZnO JRC nanoparticles. As shown in Figure 3E and Figure 3D, there is a substantial loss of cell viability at both 4h and 24h exposure. At 4h exposure, the cell viability is under 50% of control at all concentrations, with or without the presence of serum. In the case serum starvation at 24h exposure, cells have shown no viability (only 1-2% of control) at all concentrations except 15.625 µg/ml.

Recent studies have suggested ZnO nanoparticles as a possible anticancer agent due to their higher toxicity towards rapidly dividing cancer cells [101]. However, several toxicological have shown that ZnO nanoparticles significantly decrease the cell viability not only in cancer cell lines of the lung, kidney, skin, immune system, and gut but also in primary cells such as immune cells, neural stem cells, or fibroblasts [102], [103]. Other negative effects that been attributed to ZnO nanoparticles are inflammatory reactions, changed cell cycle, and DNA damage. Zinc oxide (ZnO) nanoparticles are manufactured extensively with various commercial applications, such as antibacterial coatings and UV absorbers in sunscreens and textiles. Therefore an investigation concerning their toxicity is required [102].

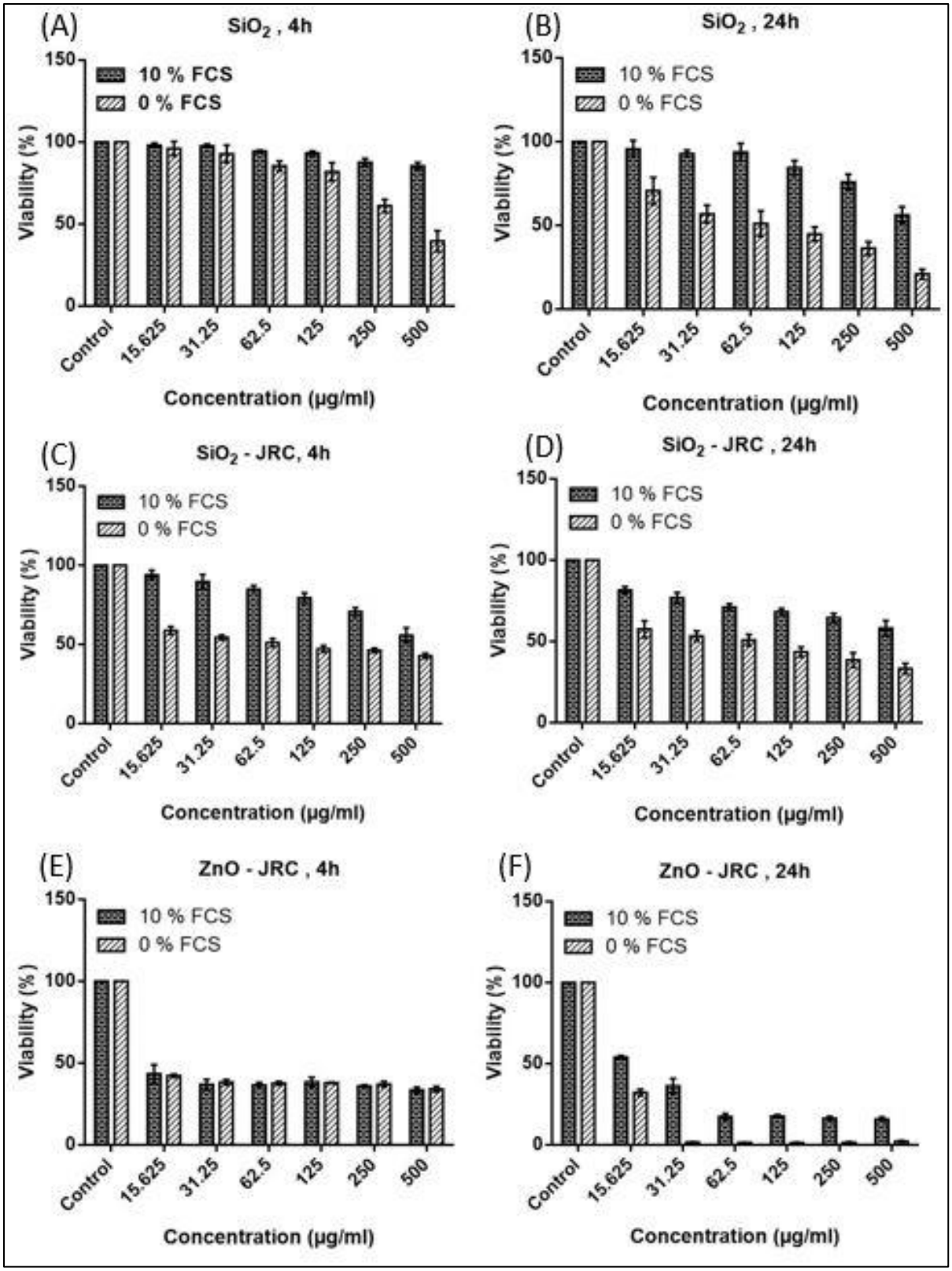

Figure 5. Toxicity assessment of SiO_2, SiO_2 JRC, and ZnO JRC nanoparticles. Cells were exposed for 4h and 24h under both 10% FCS and 0% FCS. Data are mean values ± SD (n=3).

4.2 Assessment of generated reactive oxygen species by nanoparticles

The Image-iT LIVE Green ROS detection kit has been used to detect the ROS generated by different nanoparticles and chemical compounds at different concentrations. The detection kit is based on 5-(and-6)-carboxy-2′,7′-dichlorodihydrofluorescein diacetate (carboxy-H2DCFDA), which is a reliable fluorogenic indicator for ROS generated in live cells (Figure 6) [104].

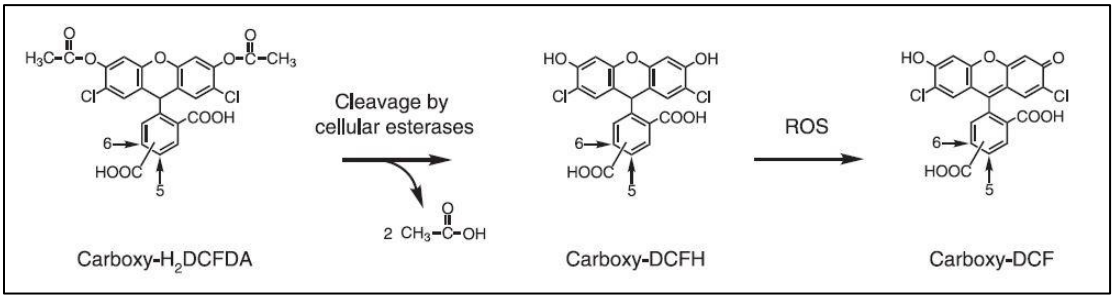

Figure 6. The nonfluorescent carboxy-H2DCFDA permeates the live cells and deacetylates by cellular esterases. In the presence of ROS generated in the cells during oxidative stress, the reduced fluorescein compound is oxidized and emits green fluorescence [104].

Additionally, the detection kit has provided *tert*-butyl hydroperoxide (TBHP), which is a common oxidant used as a positive control during nanoparticles induced toxicity via oxidative stress [105].

Chlorpromazine (CPZ) is known to induce toxicity and oxidative stress in various cells [61], [106], [107]. Therefore it was used to optimize the ROS detection protocol on bewo b30 cell line, with different concentrations, TBHP as a positive control, and negative control being the untreated cells (Figure 7). As demonstrated in Figure 7, the ROS+ (100 µM TBHP) has produced significant oxidative stress, which is visible by microscope as an emitting bright green fluorescent in comparison to the untreated control, which is almost entirely dark. Chlorpromazine (CPZ) shows oxidative stress as significant to TBHP at 150 nM and 75 nM, and with a decrease in CPZ concentrations, the emitted fluorescent is reduced, meaning that less ROS is produced by the cells, thus lower toxicity at those concentrations.

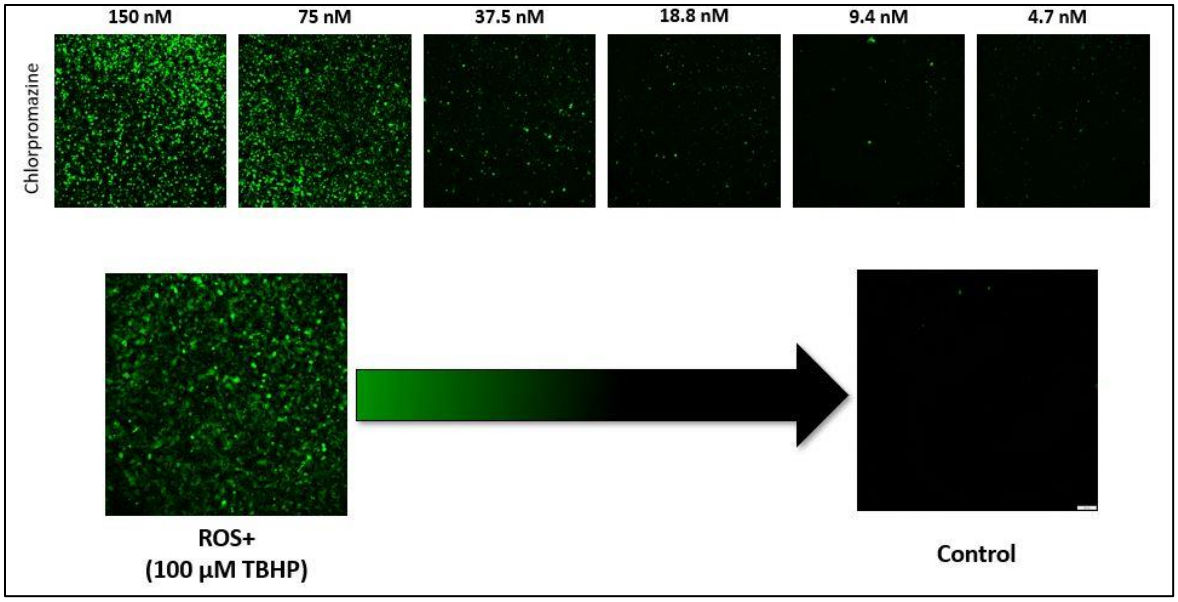

Figure 7. ROS detection in bewo b30 cells, treated with CPZ in different concentrations. 100µM of TBHP was used as ROS+ and control being untreated cells with only media.

Oxidative stress in JRC nanoparticles was investigated using the optimized ROS detection protocol. In these sets of measurements, three different JRC nanoparticles were investigated with varying concentrations with 4% FCS and at 4h exposure time. Figure 8 shows the results obtained by fluorescent microscopy. As demonstrated, ZnO JRC shows higher oxidative stress, especially at 500 µg/ml, 250 µg/ml, and 125 µg/ml and graduate decrease in ROS production at lower concentrations. TiO_2 JRC is less toxic compared to ZnO. However, it appears to generate more ROS and toxicity in comparison to SiO_2 JRC. As shown in Figure 8, with a decrease in nanoparticle concentrations, the fluorescence emission decreases significantly in both TiO_2 JRC and SiO_2 JRC.

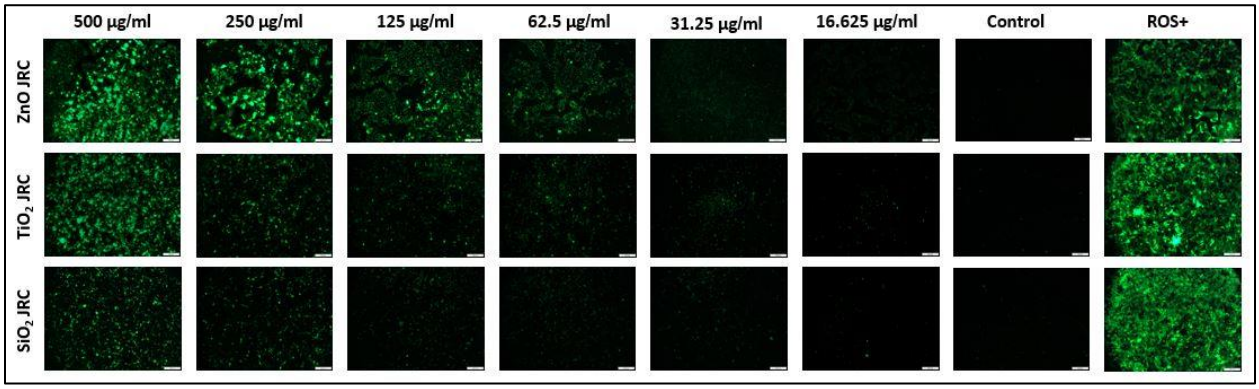

Figure 8. ROS detection in bewo b30 cells, exposed over 4h to JRC nanoparticles at different concentrations with 4% FCS. 100µM of TBHP was used as ROS+ and control being untreated cells with only media.

Furthermore, ROS production by SiO_2 ICN has been investigated at different concentrations in the presence of serum (10% FCS), as well as serum-free conditions, over 4h and 24h exposure time. As shown in Figure 9, there is high oxidative stress at 500 µg/ml, 250 µg/ml and 125 µg/ml in serum-free media at 24h exposure, meaning that both exposure time and serum play an essential rule in the toxicity of SiO_2 ICN nanoparticles. Evidently, in the case of 10% FCS in the media and 4h exposure time, nanoparticles generate less ROS, meaning lower toxicity and oxidative stress, which also correlates with the PrestoBlue results shown in Figure 5A.

These findings emphasize the importance of serum in the media while conducting toxicity assessments on nanoparticles since nanoparticles interact with biological fluids containing proteins and form protein corona. Protein corona may protect the cell membrane against the reactive surfaces of nanoparticles, and it can increase the stability of nanoparticles, thus decreasing the cellular toxicity or oxidative stress [108].

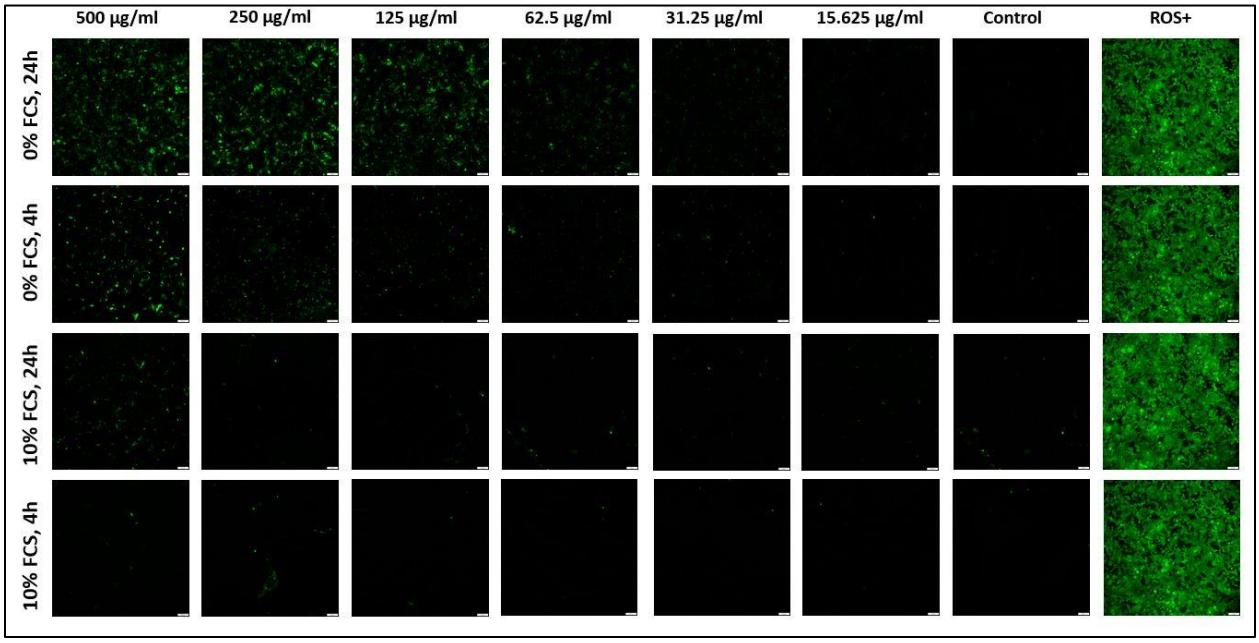

Figure 9. ROS detection in bewo b30 cells, exposed over 4h and 24h to SiO_2 ICN at different concentrations with 0% FCS and 10% FCS. 100µM of TBHP was used as ROS+ and control being untreated cells with only media.

4.3 Optimization of the microfluidic oxygen measurement setup

The microfluidic nanotoxicological system developed for continuous monitoring of cell viability consists of a microfluidic chip with integrated oxygen sensors, 3D printed interface, heating chamber, syringe pump, and FireStingO_2 optical oxygen meter (Figure 10).

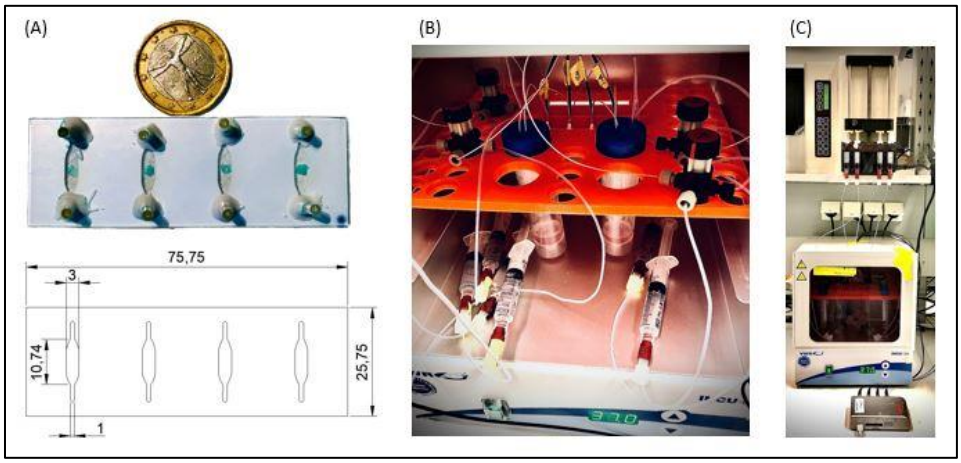

Figure 10. Microfluidic system for continuous oxygen monitoring. (A) Microfluidic chip with integrated PtTPTBPF oxygen sensors, based on microscope slides and micropatterned adhesive films. (B) 3D printed platform to mount the chip, consisting of optical fiber holder, 4-way fluid valves, and tubing. (C) Syringe pump on the top for continuous perfusion, the heating chamber at 37° C, and FireStingO_2 optical oxygen meter.

The microfluidic chip (Figure 10A) is mounted on the 3D platform (Figure 10B) with the fiber holder fixed on the chip via screws. Syringes are connected to the inlet via PEEk tubing and outlet to the 50 ml falcon tubes to contain the waste. 4-way valves are used to switch between PBS syringes (for removing bubbles and washing the chip and tubes) and perfusion syringes. The platform is placed in a heating chamber (Figure 10C) at 37° C to maintain the ideal temperature for cell culture. FireStingO_2 is connected via optical fibers through an opening on top of the heating chamber to the chip (Figure 10C).

The integrated PtTPTBPF oxygen sensors (Figure 11) is based on red-light excitation and near-infrared (NIR) emission. As demonstrated in Figure 11B, red-light excitation (620 nm) is transmitted via red light source through the optical fiber and emitted back from the oxygen sensor to the infrared detector at NIR (760 nm). The red-light sensors show luminescence in the near-infrared (NIR), which decreases with high oxygen levels and increases at low oxygen levels (Figure 11C). The phase shift between excitation and luminescence (Figure 11D) is registered

continuously by the FireStingO_2, which is the basis of measuring the oxygen consumption of cells, thus monitoring their viability.

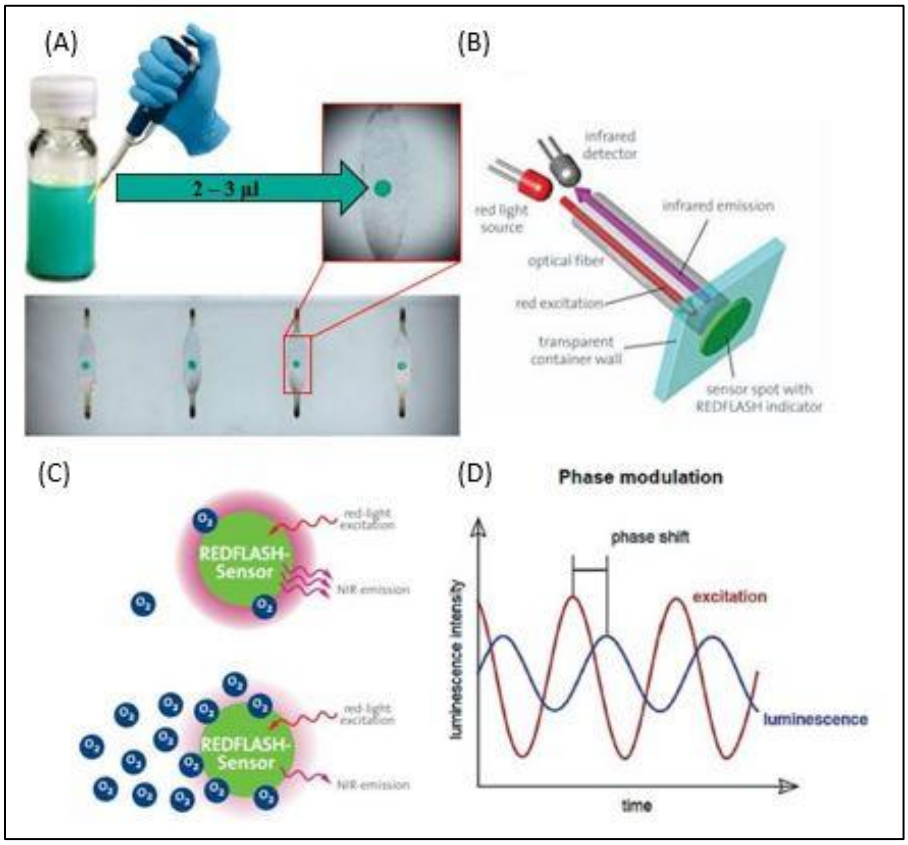

Figure 11. (A) Integrated PtTPTBPF oxygen sensors applied via pipetting on the glass. (B) Red-light excitation from the red light source and NIR emission from the sensor to the infrared detector via optical fiber [109]. (C) High NIR emission at low O_2 levels and low NIR emission at high O_2 levels [109]. (D) The phase shift between excitation and luminescence [110].

Both static and stop-flow oxygen monitoring of bewo b30 cells were conducted in this study. In order to monitor oxygen consumption of cells without a microfluidic flow, cells were seeded with three different concentrations of chlorpromazine (CPZ) and $SiO_2$2 ICN and control being only the medium. Then the oxygen consumption of the cells was monitored continuously for hours. As illustrated in Figure 12, CPZ is highly toxic at 600 nM, since there is no oxygen consumption at this concentration and partial oxygen pressure remain constant during the incubation. On the other hand, with a decrease in CPZ concentration, oxygen consumption increases, meaning cells are still viable. Similarly, the oxygen consumption of SiO_2 ICN was monitored. SiO_2 ICN appears to be less toxic in the presence of serum (10% FCS) since there was oxygen consumption at all

concentrations. However, at 500 µg/ml, the slope is less steep, indicating that oxygen consumption is slower, therefore cell viability is lower.

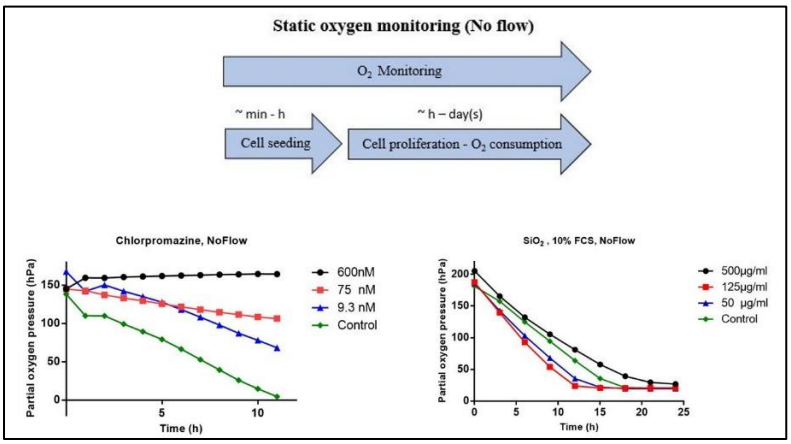

Figure 12. Static O_2 monitoring. (Bottom left) Bewo b30 cells O_2 monitoring treated with chlorpromazine. (Bottom right) Bewo b30 cells O_2 monitoring exposed to SiO_2 ICN with 10% FCS.

Another method to monitor oxygen consumption of cells and estimate their viability is the stop-flow measurement. In this method, oxygen consumption is measured in multiple stop-flow cycles. Each cycle consists of 10 minutes of flow at 10 µl/min, following with a stop of the perfusion for 5 minutes, resulting in a drop in partial oxygen pressure (Figure 13). This change in partial oxygen pressure is then used to estimate cell viability.

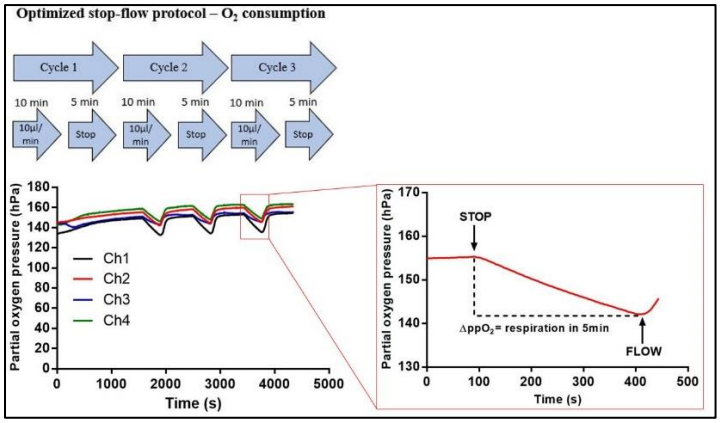

Figure 13. Optimized stop-flow protocol for monitoring oxygen consumption in a short period.

Figure 14 demonstrates the complete stop-flow processes mentioned above. Before seeding the cells, a baseline stop-flow measurement must be conducted to determine the O_2 drop of the background, which in this case, is cell culture media. Bewo b30 cells were seeded in chip and incubated overnight to form a confluent monolayer. The next step is to perform a stop-flow process before treating the cells with chlorpromazine (CPZ) to determine the oxygen consumption of healthy cells. Then cells were perfused with media containing different CPZ concentrations for 30 minutes. In the following, another stop-flow process was conducted to determine the oxygen consumption of CPZ treated cells. The data obtained from the O_2 logger application is analyzed using Matlab to calculate the change in oxygen consumption or delta. The cell viability is estimated by using delta values obtained from the measurement in the equation shown in Figure 14, and results were plotted using GraphPad. The results showed a significant decrease in cell viability at 300 nM following with cell viability around 50% at 75 nM.

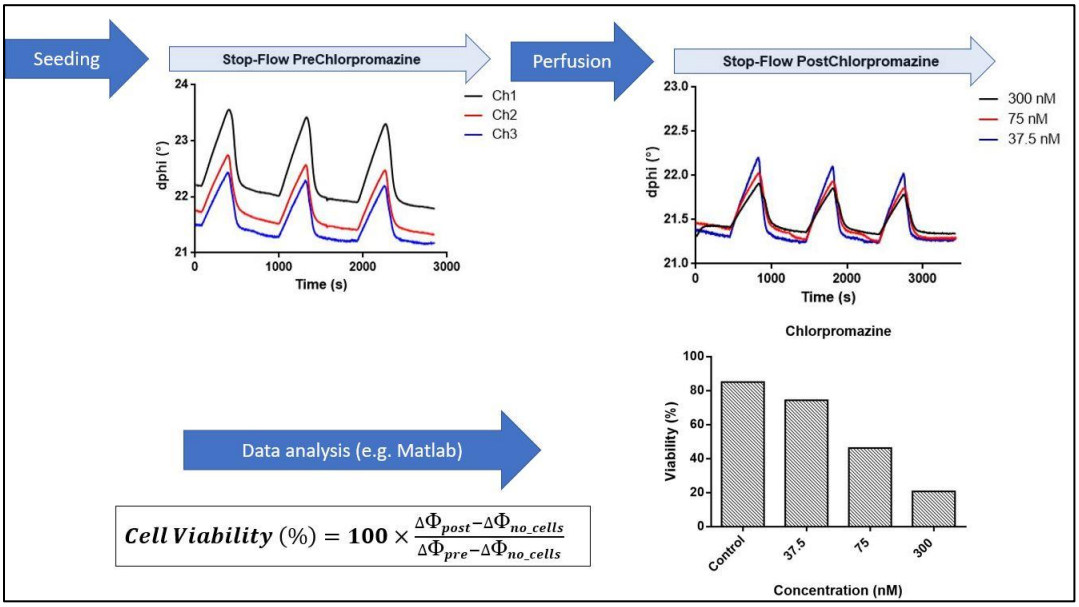

Figure 14. Complete stop-flow measurement. Bewo b30 cells were seeded and exposed to CPZ for 30 minutes. Cell viability was estimated using stop-flow delta values of pre and post-treatment. Cell viability is shown in %.

Similarly, a stop-flow measurement was conducted to investigate the toxicity of SiO_2 ICN nanoparticles on bewo b30 cells. In this case, cells were perfused with 0%FCS for 4h, and Live/Dead assay was used to evaluate further and compare the cell viability to oxygen

measurement. As shown in Figure 15, cell viability decreases significantly below 40% at the highest concentration. However, there was a difference in the Live/Dead assay compared to O_2 viability results at the control and 50 µg/ml. This difference is due to the decrease in cell number after 4h perfusion. The reduction in cell number after perfusion is one of the few drawbacks of this method. However, cells have different behavior under microfluidic flow, and some cell lines are more robust to the flow conditions and sheer-stress than others. Another challenge in this method is the appearance of air bubbles in the microfluidic chamber or on top of the oxygen sensors resulting in complications, such as cell detachment and false signals during measurements.

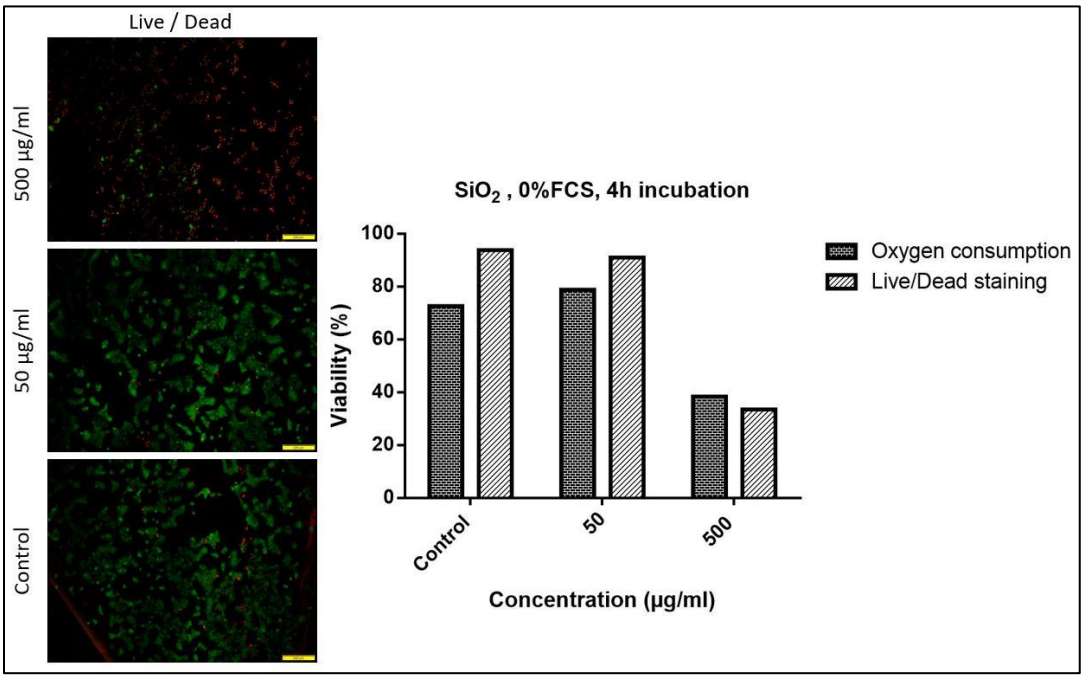

Figure 15. Bewo b30 cells exposed to SiO_2 ICN with 0%FCS for 4h. A comparison between Live/dead assay and monitoring oxygen consumption and estimating cell viability using the stop-flow method.

4.4 Matlab data analysis

The Matlab algorithm aims to automatically find three stop-flow data points from the Excel file generated by the O_2 logger and calculate delta, mean, and standard deviation for each channel and plot the graphs for the given time. The output result will be saved as an Excel file.

During the measurement, comments must be added to pinpoint the stop-flow initiation in the data file. Comments must be lower case, and space must be avoided (e.g., stop1, stop2,stop3).

After stoping the O_2 logger application and finishing the measurement, the algorithm generates a text file. The text file was copied in Excel and moved to the Matlab directory (current) folder. The file name must be entered between apostrophes in line 6, without and file extension, to load the excel file in Matlab (Figure 16). The comments must be added respectively between apostrophes at line 9, line 75, and line 141, In this case, stop1,stop2, and stop3 (Figure 16). Next, the stop-flow duration time (in seconds) must be adjusted in line12, line 78, and line 144. In this case, the stop-flow is 3 minutes or 180 seconds (Figure 16).

```
1
2 -    clear
3 -    clc
4 -    close all
5
6 -    [data,text,raw]=xlsread('green_channel3and4_day2_preNP');% Load Excell file
7      %%%%%%%%%R%E%Z%A%%%%%A%F%K%H%M%I%%%%%%%%%%%%%%%%%%%%%%%%%%%%%%%%%%%%%%%%
8      %Stop Flow 1
9 -    x_s1=strcmpi(text(:,4),'stop1'); %the comment that we are looking for
10 -   c_s1=find(x_s1==1);
11 -   d1_s1=c_s1-4; %row number in data
12 -   d2_s1=d1_s1+180; %row after 180 seconds
13
14     %Channel 1
15 -   ch1v1_s1=data(d1_s1,4); %channel 1 value 1
16 -   ch1v2_s1=data(d2_s1,4); %channel 1 value 2 ,e.g. after 2min
17 -   D1_s1=ch1v1_s1-ch1v2_s1; %Delta
18 -   S1_s1=std(data(d1_s1:d2_s1,4)); %Standard deviation
19 -   M1_s1=mean(data(d1_s1:d2_s1,4)); %Mean
20 -   figure
21 -   plot(data(d1_s1:d2_s1,4),'LineWidth',2)
22 -   title('Stop Flow 1')
23 -   hold on
24
```

Figure 16. Matlab algorithm. Loading excel file and adjusting comments and time.

After executing the program, the oxygen uptake and respiration for 3 minutes are plotted (Figure 17). Furthermore, the delta between the beginning and end of the stop-flow, mean, and standard deviation of each channel are calculated and saved as an excel file that can be found in the Matlab directory folder.

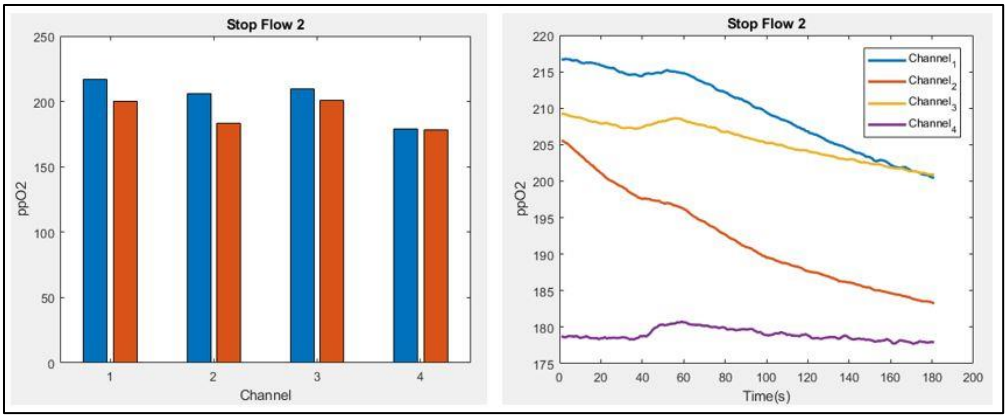

Figure 17. Respiration and oxygen uptake during a stop-flow cycle

Based on the delta values obtained by the algorithm, eventually, the viability of the cells could be calculated using the following equation:

$$\boldsymbol{Cell\ Viability}\ (\%) = \mathbf{100} \times \frac{\Delta\Phi_{\boldsymbol{post}} - \Delta\Phi_{\boldsymbol{no\_cells}}}{\Delta\Phi_{\boldsymbol{pre}} - \Delta\Phi_{\boldsymbol{no\_cells}}}$$

Matlab provides a vast and robust set of tools and formulas to analyze the data and robust data visualization to generate and modify plots and graphs. Matlab code could be potentially compiled and converted to other programming languages such as python for more optimization in the code and the performance.

4.5 Proof of concept on the single-cell microarray

The single-cell microarray (Figure 18) aims to immobilize and capture single cells, which allows specific analysis to be performed on individual cells. The chip consists of 86 cell traps, each with 6µm width. Bewo b30 cells were diluted and loaded in the cells with a syringe to assess the trapping efficiency of the chip. Cells were trapped in around 50% in the best case, with some chips entirely clogged by the cells at the inlet.

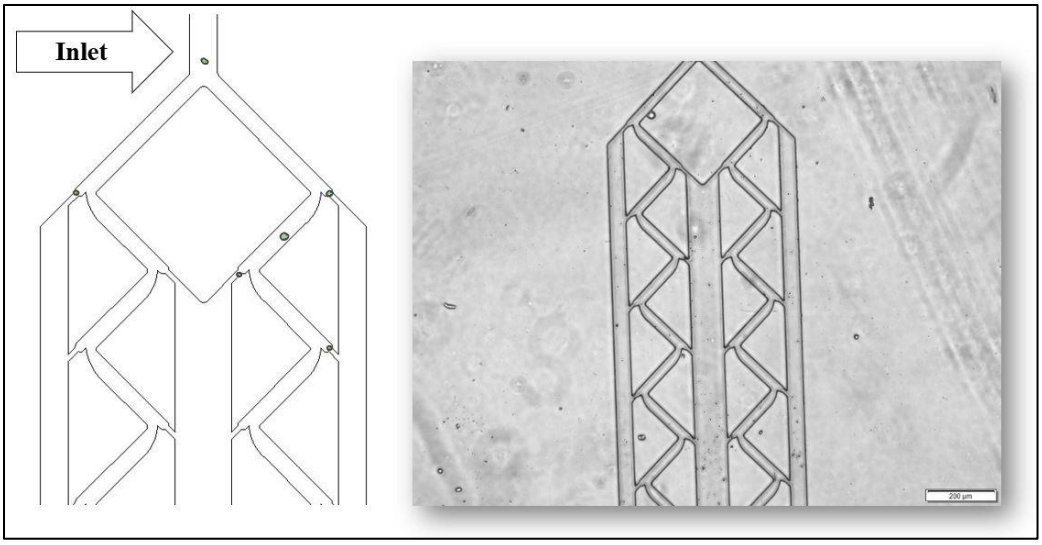

Figure 18. (Left) Schematic demonstration of the single-cell chip. (Right) Microscope image of the PDMS chip.

After capturing the bewo b30 cells, the microarrays were exposed to chlorpromazine and SiO_2 ICN nanoparticles to investigate their toxicity on induvial cells. Figure 19 demonstrates the trapped bewo b30 cells treated with chlorpromazine for 30 minutes, following with ethidium bromide staining to indicating the dead cells.

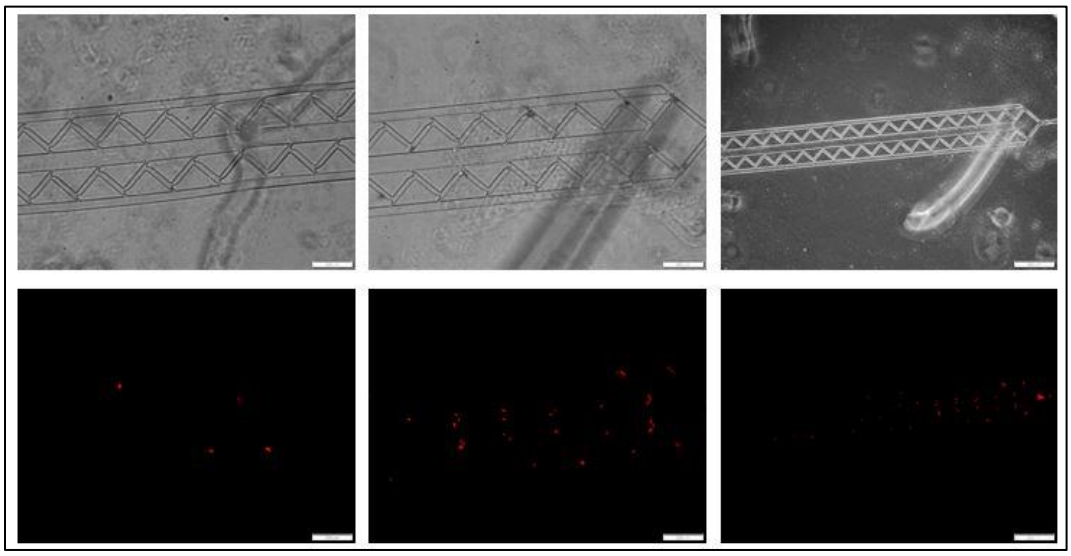

Figure 19. Bewo b30 cells trapped in the microarray and treated with CPZ for 30 minutes. Dead cells were stained using ethidium bromide.

Similarly, bewo cells were exposed to SiO_2 ICN nanoparticles with 0%FCS for 4h. After the incubation, cells were stained with ethidium bromide to demonstrate the dead cells.

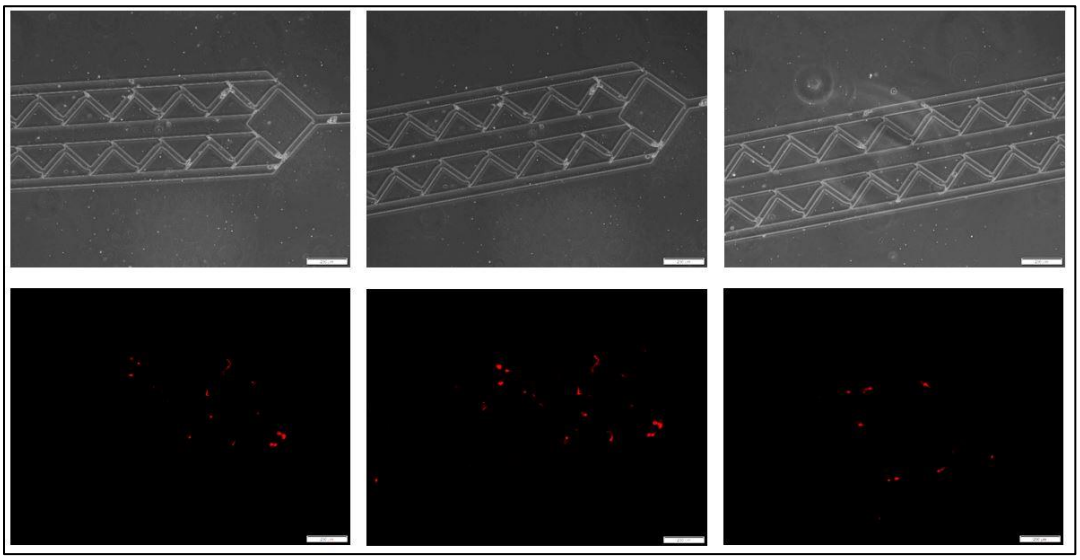

Figure 20. Bewo b30 cells captured and exposed to SiO_2 ICN nanoparticles with 0%FCS for 4h. Dead cells were stained using ethidium bromide.

5 Conclusion

The PrestoBlue and ROS detection assays were used to assess the toxicity of different nanoparticles at different concentrations, exposure time, as well as under serum starvation conditions. The toxicity of nanoparticles has increased in serum-free media and longer exposure time. Moreover, SiO_2 JRC has shown more toxicity and reactivity compared to SiO_2 ICN, meaning that JRC nanoparticles have different physicochemical properties that influence their reactivity and nanotoxicity.

To further investigate the toxicity of nanoparticles, a microfluidic nanotoxicological system with integrated oxygen sensors has been developed. The microfluidic chip is based on microscope slides and biocompatible micropatterned adhesive films, which provides rapid prototyping and development of the chip.

The Oxygen sensors are applied directly via pipetting, resulting in effortless sensor integration. These sensors are label-free and non-invasive, meaning that they are suitable for continuous monitoring of oxygen levels in cell culture. Both static and stop-flow oxygen monitoring methods were used to assess the toxicity of chlorpromazine and SiO_2 ICN. In the case of static monitoring, oxygen levels were measured continuously for hours, rendering an estimation of overall cell respiration and viability. On the other hand, stop-flow measurements were conducted under short period, resulting in a fast response of the sensors to oxygen consumption in the presence of cellular respiration in viable cells.

The proof of concept for a single-cell microarray has been provided. The single-cell microarray is PDMS based chip capable of trapping single cells, which can be utilized to analyze individual cells. Bewo b30 cells were trapped in the microarray and exposed to chlorpromazine and nanoparticles to evaluate their induced toxicity on individual cells.

References

[1] T. G. Smijs and S. Pavel, "Titanium dioxide and zinc oxide nanoparticles in sunscreens: Focus on their safety and effectiveness," *Nanotechnol. Sci. Appl.*, vol. 4, no. 1, pp. 95–112, 2011.

[2] A. Bitar, N. M. Ahmad, H. Fessi, and A. Elaissari, "Silica-based nanoparticles for biomedical applications," *Drug Discov. Today*, vol. 17, no. 19–20, pp. 1147–1154, 2012.

[3] Y. Cui, Q. Wei, H. Park, and C. M. Lieber, "Nanowire nanosensors for highly sensitive and selective detection of biological and chemical species," *Science (80-.).*, vol. 293, no. 5533, pp. 1289–1292, 2001.

[4] P. R. Nair and M. A. Alam, "Design considerations of silicon nanowire biosensors," *IEEE Trans. Electron Devices*, vol. 54, no. 12, pp. 3400–3408, 2007.

[5] A. El-Ansary and S. Al-Daihan, "On the Toxicity of Therapeutically Used Nanoparticles: An Overview," *J. Toxicol.*, vol. 2009, pp. 1–9, 2009.

[6] S. K. Mahto, V. Charwat, P. Ertl, B. Rothen-Rutishauser, S. W. Rhee, and J. Sznitman, "Microfluidic platforms for advanced risk assessments of nanomaterials," *Nanotoxicology*, vol. 9, no. 3, pp. 381–395, 2015.

[7] P. J. A. Borm *et al.*, *The potential risks of nanomaterials: A review carried out for ECETOC*, vol. 3. 2006.

[8] R. Landsiedel *et al.*, "Testing metal-oxide nanomaterials for human safety," *Adv. Mater.*, vol. 22, no. 24, pp. 2601–2627, 2010.

[9] X. Liu, D. Wang, and Y. Li, "Synthesis and catalytic properties of bimetallic nanomaterials with various architectures," *Nano Today*, vol. 7, no. 5, pp. 448–466, 2012.

[10] B. S. Murty, P. Shankar, B. Raj, B. B. Rath, and J. Murday, *Textbook of Nanoscience and Nanotechnology*, vol. d. 2013.

[11] H. F. Krug and P. Wick, "Nanotoxicology: An interdisciplinary challenge," *Angew. Chemie - Int. Ed.*, vol. 50, no. 6, pp. 1260–1278, 2011.

[12] A. E. Nel *et al.*, "Understanding biophysicochemical interactions at the nano-bio interface," *Nat. Mater.*, vol. 8, no. 7, pp. 543–557, 2009.

[13] D. J. Betteridge, "What is oxidative stress?," *Metabolism.*, vol. 49, no. 2 SUPPL. 1, pp. 3–8, 2000.

[14] S. C. McCormick *et al.*, "The use of microfluidics in cytotoxicity and nanotoxicity experiments," *Micromachines*, vol. 8, no. 4, pp. 1–18, 2017.

[15] T. Finkel and N. J. Holbrook, "Oxidants, oxidative stress and the biology of ageing," *Nature*, vol. 408, no. 6809, pp. 239–247, 2000.

[16] Z. Chen *et al.*, "Acute toxicological effects of copper nanoparticles in vivo," *Toxicol. Lett.*, vol. 163, no. 2, pp. 109–120, 2006.

[17] H. Meng *et al.*, "Ultrahigh reactivity provokes nanotoxicity: Explanation of oral toxicity of nano-copper particles," *Toxicol. Lett.*, vol. 175, no. 1–3, pp. 102–110, 2007.

[18] Y. Ye, J. Liu, J. Xu, L. Sun, M. Chen, and M. Lan, "Nano-SiO 2 induces apoptosis via activation of p53 and Bax mediated by oxidative stress in human hepatic cell line," *Toxicol. Vitr.*, vol. 24, no. 3, pp. 751–758, 2010.

[19] M. Ahamed, "Silica nanoparticles-induced cytotoxicity, oxidative stress and apoptosis in cultured A431 and A549 cells," *Hum. Exp. Toxicol.*, vol. 32, no. 2, pp. 186–195, 2013.

[20] E. J. Park, J. Yi, K. H. Chung, D. Y. Ryu, J. Choi, and K. Park, "Oxidative stress and apoptosis induced by titanium dioxide nanoparticles in cultured BEAS-2B cells," *Toxicol.*

Lett., vol. 180, no. 3, pp. 222–229, 2008.
[21] K. S. Ko and I. C. Kong, "Toxic effects of nanoparticles on bioluminescence activity, seed germination, and gene mutation," *Appl. Microbiol. Biotechnol.*, vol. 98, no. 7, pp. 3295–3303, 2014.
[22] I. Lynch and K. A. Dawson, "Protein-nanoparticle interactions," *Nano Today*, vol. 3, no. 1–2, pp. 40–47, 2008.
[23] I. Lynch, T. Cedervall, M. Lundqvist, C. Cabaleiro-Lago, S. Linse, and K. A. Dawson, "The nanoparticle-protein complex as a biological entity; a complex fluids and surface science challenge for the 21st century," *Adv. Colloid Interface Sci.*, vol. 134–135, pp. 167–174, 2007.
[24] J. H. Moran and R. G. Schnellmann, "A rapid β-NADH-linked fluorescence assay for lactate dehydrogenase in cellular death," *J. Pharmacol. Toxicol. Methods*, vol. 36, no. 1, pp. 41–44, Sep. 1996.
[25] J. Zhao and V. Castranova, "Toxicology of Nanomaterials Used in Nanomedicine," *J. Toxicol. Environ. Heal. Part B*, vol. 14, no. 8, pp. 593–632, Nov. 2011.
[26] T. Wang, J. Bai, X. Jiang, and G. U. Nienhaus, "Cellular uptake of nanoparticles by membrane penetration: A study combining confocal microscopy with FTIR spectroelectrochemistry," *ACS Nano*, vol. 6, no. 2, pp. 1251–1259, 2012.
[27] P. JANI, G. W. HALBERT, J. LANGRIDGE, and A. T. FLORENCE, "Nanoparticle Uptake by the Rat Gastrointestinal Mucosa: Quantitation and Particle Size Dependency," *J. Pharm. Pharmacol.*, vol. 42, no. 12, pp. 821–826, 1990.
[28] W. G. Kreyling, S. Hirn, and C. Schleh, "Nanoparticles in the lung," *Nat. Biotechnol.*, vol. 28, no. 12, pp. 1275–1276, 2010.
[29] Y. Guo, E. Terazzi, R. Seemann, J. B. Fleury, and V. A. Baulin, "Direct proof of spontaneous translocation of lipid-covered Hydrophobic nanoparticles through a phospholipid bilayer," *Sci. Adv.*, vol. 2, no. 11, pp. 38–40, 2016.
[30] H. Kettiger, A. Schipanski, P. Wick, and J. Huwyler, "Engineered nanomaterial uptake and tissue distribution: From cell to organism," *Int. J. Nanomedicine*, vol. 8, pp. 3255–3269, 2013.
[31] P. H. Yang, X. Sun, J. F. Chiu, H. Sun, and Q. Y. He, "Transferrin-mediated gold nanoparticle cellular uptake," *Bioconjug. Chem.*, vol. 16, no. 3, pp. 494–496, 2005.
[32] N. Oh and J. H. Park, "Endocytosis and exocytosis of nanoparticles in mammalian cells," *Int. J. Nanomedicine*, vol. 9, no. SUPPL.1, pp. 51–63, 2014.
[33] M. Geiser *et al.*, "Ultrafine particles cross cellular membranes by nonphagocytic mechanisms in lungs and in cultured cells," *Environ. Health Perspect.*, vol. 113, no. 11, pp. 1555–1560, 2005.
[34] B. M. Rothen-Rutishauser, S. Schürch, B. Haenni, N. Kapp, and P. Gehr, "Interaction of fine particles and nanoparticles with red blood cells visualized with advanced microscopic techniques," *Environ. Sci. Technol.*, vol. 40, no. 14, pp. 4353–4359, 2006.
[35] A. Beduneau *et al.*, "Facilitated monocyte-macrophage uptake and tissue distribution of superparmagnetic iron-oxide nanoparticles," *PLoS One*, vol. 4, no. 2, pp. 1–12, 2009.
[36] Y. Yang *et al.*, "The biodistribution of self-assembling protein nanoparticles shows they are promising vaccine platforms," *J. Nanobiotechnology*, vol. 11, no. 1, pp. 1–10, 2013.
[37] A. J. Cole, A. E. David, J. Wang, C. J. Galbán, and V. C. Yang, "Magnetic brain tumor targeting and biodistribution of long-circulating PEG-modified, cross-linked starch-coated iron oxide nanoparticles," *Biomaterials*, vol. 32, no. 26, pp. 6291–6301, 2011.

[38] H. C. Fischer and W. C. Chan, “Nanotoxicity: the growing need for in vivo study,” *Curr. Opin. Biotechnol.*, vol. 18, no. 6, pp. 565–571, 2007.
[39] P. Kolhar, N. Doshi, and S. Mitragotri, “Polymer nanoneedle-mediated intracellular drug delivery,” *Small*, vol. 7, no. 14, pp. 2094–2100, 2011.
[40] N. M. Gude, C. T. Roberts, B. Kalionis, and R. G. King, “Growth and function of the normal human placenta,” 2004.
[41] H. N. Jones, T. L. Powell, and T. Jansson, “Regulation of Placental Nutrient Transport e A Review,” vol. 28, 2007.
[42] S. Lager and T. L. Powell, “Regulation of Nutrient Transport across the Placenta,” vol. 2012, 2012.
[43] J. S. Lee, R. Romero, Y. M. Han, H. C. Kim, C. J. Kim, and J. Hong, “Placenta-on-a-chip : a novel platform to study the biology of the human placenta,” *J. Matern. Neonatal Med.*, vol. 00, no. 00, pp. 1–9, 2015.
[44] M. Rothbauer, N. Patel, H. Gondola, and M. Siwetz, “A comparative study of five physiological key parameters between four different human trophoblast-derived cell lines,” *Sci. Rep.*, no. April, pp. 1–11, 2017.
[45] C. Blundell *et al.*, “Placental Drug Transport-on-a-Chip : A Microengineered In Vitro Model of Transporter-Mediated Drug Efflux in the Human Placental Barrier,” vol. 1700786, pp. 1–9, 2017.
[46] G. T. Knipp, K. L. Audus, and M. J. Soares, “Nutrient transport across the placenta,” vol. 38, pp. 41–58, 1999.
[47] C. P. Sibley, P. Brownbill, M. Dilworth, and J. D. Glazier, “Review : Adaptation in placental nutrient supply to meet fetal growth demand : Implications for programming,” *Placenta*, vol. 31, pp. S70–S74, 2010.
[48] A. M. Carter, “Evolution of Factors Affecting Placental Oxygen Transfer,” *Placenta*, vol. 30, pp. 19–25, 2009.
[49] F. Gaccioli, S. Lager, T. L. Powell, and T. Jansson, “Placental transport in response to altered maternal nutrition,” vol. 4, pp. 101–115, 2013.
[50] H. Kiss and P. Husslein, “Hypoxia Downregulates Continuous and Interleukin-l-induced Expression of Human Chorionic Gonadotropin in Choriocarcinoma,” pp. 597–604, 1997.
[51] T. Sivasubramaniyam *et al.*, “Where Polarity Meets Fusion : Role of Par6 in Trophoblast Differentiation during Placental Development and Preeclampsia,” vol. 154, no. March, pp. 1296–1309, 2013.
[52] P. Wick *et al.*, “Barrier Capacity of Human Placenta for Nanosized Materials,” no. 3, pp. 432–436, 2010.
[53] M. Lacasan, “Exposure to ambient air pollution and prenatal and early childhood health effects,” no. December 2003, pp. 183–199, 2005.
[54] A. Huss, C. E. Kuehni, U. Frey, P. Latzin, and M. Ro, “Air pollution during pregnancy and lung function in newborns: a birth cohort study,” vol. 33, no. 3, pp. 594–603, 2009.
[55] H. Bové *et al.*, “Ambient black carbon particles reach the fetal side of human placenta,” *Nat. Commun.*, no. 2019, pp. 1–7.
[56] E. D. Kuempel, C. L. Tran, V. Castranova, and A. J. Bailer, “Lung Dosimetry and Risk Assessment of Nanoparticles: Evaluating and Extending Current Models in Rats and Humans,” *Inhal. Toxicol.*, vol. 18, no. 10, pp. 717–724, Jan. 2006.
[57] J. McKim Jr., “Building a Tiered Approach to In Vitro Predictive Toxicity Screening: A Focus on Assays with In Vivo Relevance,” *Comb. Chem. High Throughput Screen.*, vol.

13, no. 2, pp. 188–206, 2010.
[58] X. Han *et al.*, “Assessing the relevance of in vitro studies in nanotoxicology by examining correlations between in vitro and in vivo data,” *Toxicology*, vol. 297, no. 1, pp. 1–9, 2012.
[59] V. Stone, H. Johnston, and R. P. F. Schins, “Development of in vitro systems for nanotoxicology: Methodological considerations in vitro methods for nanotoxicology Vicki Stone et al.,” *Crit. Rev. Toxicol.*, vol. 39, no. 7, pp. 613–626, 2009.
[60] T. F. Guerin, M. Mondido, B. McClenn, and B. Peasley, “Application of resazurin for estimating abundance of contaminant-degrading micro-organisms,” *Lett. Appl. Microbiol.*, vol. 32, no. 5, pp. 340–345, 2001.
[61] K. Morgan *et al.*, “Chlorpromazine toxicity is associated with disruption of cell membrane integrity and initiation of a pro-inflammatory response in the HepaRG hepatic cell line,” *Biomed. Pharmacother.*, vol. 111, no. January, pp. 1408–1416, 2019.
[62] K. Helm *et al.*, “In Vitro Cell Death Discrimination and Screening Method by Simple and Cost-Effective Viability Analysis,” *Cell. Physiol. Biochem.*, vol. 41, no. 3, pp. 1011–1019, 2017.
[63] F. Dal Yontem, S. H. Kim, Z. Ding, E. Grimm, S. Ekmekcioglu, and H. Akcakaya, “Mitochondrial dynamic alterations regulate melanoma cell progression,” *J. Cell. Biochem.*, vol. 120, no. 2, pp. 2098–2108, 2019.
[64] C. Albrecht *et al.*, “The crucial role of particle surface reactivity in respirable quartz-induced reactive oxygen/nitrogen species formation and APE/Ref-1 induction in rat lung,” *Respir. Res.*, vol. 6, pp. 1–16, 2005.
[65] V. Stone, J. Shaw, D. M. Brown, W. MacNee, S. P. Faux, and K. Donaldson, “The role of oxidative stress in the prolonged inhibitory effect of ultrafine carbon black on epithelial cell function,” *Toxicol. Vitr.*, vol. 12, no. 6, pp. 649–659, 1998.
[66] L. Foucaud, M. R. Wilson, D. M. Brown, and V. Stone, “Measurement of reactive species production by nanoparticles prepared in biologically relevant media,” *Toxicol. Lett.*, vol. 174, no. 1, pp. 1–9, 2007.
[67] K. Faulkner and I. Fridovich, “Luminol and lucigenin as detectors for O2ṡ−,” *Free Radic. Biol. Med.*, vol. 15, no. 4, pp. 447–451, 1993.
[68] O. Myhre, J. M. Andersen, H. Aarnes, and F. Fonnum, “Evaluation of the probes 2′,7′-dichlorofluorescin diacetate, luminol, and lucigenin as indicators of reactive species formation,” *Biochem. Pharmacol.*, vol. 65, no. 10, pp. 1575–1582, 2003.
[69] P. Haberzettl, R. P. F. Schins, D. Höhr, V. Wilhelmi, P. J. A. Borm, and C. Albrecht, “Impact of the FcγII-receptor on quartz uptake and inflammatory response by alveolar macrophages,” *Am. J. Physiol. - Lung Cell. Mol. Physiol.*, vol. 294, no. 6, 2008.
[70] N. A. Monteiro-Riviere, A. O. Inman, and L. W. Zhang, “Limitations and relative utility of screening assays to assess engineered nanoparticle toxicity in a human cell line,” *Toxicol. Appl. Pharmacol.*, vol. 234, no. 2, pp. 222–235, 2009.
[71] J. M. Balbus *et al.*, “Meeting report: Hazard assessment for nanoparticles-report from an interdisciplinary workshop,” *Environ. Health Perspect.*, vol. 115, no. 11, pp. 1654–1659, 2007.
[72] J. M. Wörle-Knirsch, K. Kern, C. Schleh, C. Adelhelm, C. Feldmann, and H. F. Krug, “Nanoparticulate vanadium oxide potentiated vanadium toxicity in human lung cells,” *Environ. Sci. Technol.*, vol. 41, no. 1, pp. 331–336, 2007.
[73] A. Nel, T. Xia, L. Mädler, and N. Li, “Toxic Potential of Materials at the Nanolevel,” *Science (80-.).*, vol. 311, no. 5761, pp. 622 LP – 627, Feb. 2006.

[74] G. Oberdörster, E. Oberdörster, and J. Oberdörster, "Nanotoxicology: An emerging discipline evolving from studies of ultrafine particles," *Environ. Health Perspect.*, vol. 113, no. 7, pp. 823–839, 2005.
[75] D. Erickson and D. Li, "Integrated microfluidic devices," *Anal. Chim. Acta*, vol. 507, no. 1, pp. 11–26, 2004.
[76] P. Abgrall and A. M. Gué, "Lab-on-chip technologies: Making a microfluidic network and coupling it into a complete microsystem - A review," *J. Micromechanics Microengineering*, vol. 17, no. 5, 2007.
[77] P. S. Dittrich and A. Manz, "Lab-on-a-chip: Microfluidics in drug discovery," *Nat. Rev. Drug Discov.*, vol. 5, no. 3, pp. 210–218, 2006.
[78] J. P. Puccinelli, X. su, and D. J. Beebe, "Automated High-Throughput Microchannel Assays for Cell Biology: Operational Optimization and Characterization," *J. Lab. Autom.*, vol. 15, no. 1, pp. 25–32, 2010.
[79] S. M. Grist, L. Chrostowski, and K. C. Cheung, "Optical oxygen sensors for applications in microfluidic cell culture," *Sensors (Switzerland)*, vol. 10, no. 10, pp. 9286–9316, 2010.
[80] S. K. Mahto, T. H. Yoon, and S. W. Rhee, "A new perspective on in vitro assessment method for evaluating quantum dot toxicity by using microfluidics technology," *Biomicrofluidics*, vol. 4, no. 3, p. 34111, Sep. 2010.
[81] D. Kim, Y. S. Lin, and C. L. Haynes, "On-chip evaluation of shear stress effect on cytotoxicity of mesoporous silica nanoparticles," *Anal. Chem.*, vol. 83, no. 22, pp. 8377–8382, 2011.
[82] C. A. Cunha-Matos, O. M. Millington, A. W. Wark, and M. Zagnoni, "Real-time multimodal imaging of nanoparticle-cell interactions in high-throughput microfluidics," *18th Int. Conf. Miniaturized Syst. Chem. Life Sci. MicroTAS 2014*, no. November 2015, pp. 968–970, 2014.
[83] M. Rothbauer, I. Praisler, D. Docter, R. H. Stauber, and P. Ertl, "Microfluidic impedimetric cell regeneration assay to monitor the enhanced cytotoxic effect of nanomaterial perfusion," *Biosensors*, vol. 5, no. 4, pp. 736–749, 2015.
[84] L. Jagannathan, S. Cuddapah, and M. Costa, "Oxidative Stress Under Ambient and Physiological Oxygen Tension in Tissue Culture," *Curr. Pharmacol. Reports*, vol. 2, no. 2, pp. 64–72, 2016.
[85] J. J. P. Gille and H. Joenje, "Cell culture models for oxidative stress: superoxide and hydrogen peroxide versus normobaric hyperoxia," *Mutat. Res. DNAging*, vol. 275, no. 3–6, pp. 405–414, 1992.
[86] M. S. Goligorsky, "Making sense out of oxygen sensor," *Circ. Res.*, vol. 86, no. 8, pp. 824–826, 2000.
[87] M. Csete, "Oxygen in the cultivation of stem cells," *Ann. N. Y. Acad. Sci.*, vol. 1049, pp. 1–8, 2005.
[88] M. G. Nichols and T. H. Foster, "Oxygen diffusion and reaction kinetics in the photodynamic therapy of multicell tumour spheroids," *Phys. Med. Biol.*, vol. 39, no. 12, pp. 2161–2181, 1994.
[89] A. Weltin *et al.*, "Cell culture monitoring for drug screening and cancer research: A transparent, microfluidic, multi-sensor microsystem," *Lab Chip*, vol. 14, no. 1, pp. 138–146, 2014.
[90] J. Ehgartner *et al.*, "Online analysis of oxygen inside silicon-glass microreactors with integrated optical sensors," *Sensors Actuators, B Chem.*, vol. 228, pp. 748–757, 2016.

[91] X. D. Wang and O. S. Wolfbeis, “Optical methods for sensing and imaging oxygen: Materials, spectroscopies and applications,” *Chem. Soc. Rev.*, vol. 43, no. 10, pp. 3666–3761, 2014.
[92] L. C. Lasave, S. M. Borisov, J. Ehgartner, and T. Mayr, “Quick and simple integration of optical oxygen sensors into glass-based microfluidic devices,” *RSC Adv.*, vol. 5, no. 87, pp. 70808–70816, 2015.
[93] S. Sun, B. Ungerböck, and T. Mayr, “Imaging of oxygen in microreactors and microfluidic systems,” *Methods Appl. Fluoresc.*, vol. 3, no. 3, 2015.
[94] H. Zirath *et al.*, “Every breath you take: Non-invasive real-time oxygen biosensing in two- and three-dimensional microfluidic cell models,” *Front. Physiol.*, vol. 9, no. JUL, pp. 1–12, 2018.
[95] P. Gruber, M. P. C. Marques, N. Szita, and T. Mayr, “Integration and application of optical chemical sensors in microbioreactors,” *Lab Chip*, vol. 17, no. 16, pp. 2693–2712, 2017.
[96] B. Ungerböck, V. Charwat, P. Ertl, and T. Mayr, “Microfluidic oxygen imaging using integrated optical sensor layers and a color camera,” *Lab Chip*, vol. 13, no. 8, pp. 1593–1601, 2013.
[97] J. Ehgartner, H. Wiltsche, S. M. Borisov, and T. Mayr, “Low cost referenced luminescent imaging of oxygen and pH with a 2-CCD colour near infrared camera,” *Analyst*, vol. 139, no. 19, pp. 4924–4933, 2014.
[98] P. E. Oomen, M. D. Skolimowski, and E. Verpoorte, “Implementing oxygen control in chip-based cell and tissue culture systems,” *Lab Chip*, vol. 16, no. 18, pp. 3394–3414, 2016.
[99] J. Shi *et al.*, “Microsomal glutathione transferase 1 protects against toxicity induced by silica nanoparticles but not by zinc oxide nanoparticles,” *ACS Nano*, vol. 6, no. 3, pp. 1925–1938, 2012.
[100] L. Farcal *et al.*, “Comprehensive in vitro toxicity testing of a panel of representative oxide nanomaterials: First steps towards an intelligent testing strategy,” *PLoS One*, vol. 10, no. 5, pp. 1–34, 2015.
[101] J. W. Rasmussen, E. Martinez, P. Louka, and D. G. Wingett, “Zinc oxide nanoparticles for selective destruction of tumor cells and potential for drug delivery applications,” *Expert Opin. Drug Deliv.*, vol. 7, no. 9, pp. 1063–1077, 2010.
[102] T. Buerki-Thurnherr *et al.*, “In vitro mechanistic study towards a better understanding of ZnO nanoparticle toxicity,” *Nanotoxicology*, vol. 7, no. 4, pp. 402–416, Jun. 2013.
[103] S. Tuomela *et al.*, “Gene Expression Profiling of Immune-Competent Human Cells Exposed to Engineered Zinc Oxide or Titanium Dioxide Nanoparticles,” *PLoS One*, vol. 8, no. 7, 2013.
[104] Q. Facts, “MP 36007 Image-iT ™ LIVE Green Reactive Oxygen Species Detection Kit Product Information,” pp. 1–3, 2004.
[105] D. M. Brown, L. Hutchison, K. Donaldson, S. J. MacKenzie, C. A. J. Dick, and V. Stone, “The effect of oxidative stress on macrophages and lung epithelial cells: The role of phosphodiesterases 1 and 4,” *Toxicol. Lett.*, vol. 168, no. 1, pp. 1–6, 2007.
[106] T. Li, Q. Zhou, N. Zhang, and Y. Luo, “Toxic effects of chlorpromazine on Carassius auratus and its oxidative stress,” *J. Environ. Sci. Heal. Part B*, vol. 43, no. 8, pp. 638–643, Nov. 2008.
[107] S. Ficarra, A. Russo, D. Barreca, E. Giunta, A. Galtieri, and E. Tellone, “Short-Term

Effects of Chlorpromazine on Oxidative Stress in Erythrocyte Functionality: Activation of Metabolism and Membrane Perturbation," *Oxid. Med. Cell. Longev.*, vol. 2016, 2016.
[108] C. Corbo, R. Molinaro, A. Parodi, N. E. Toledano Furman, F. Salvatore, and E. Tasciotti, "The impact of nanoparticle protein corona on cytotoxicity, immunotoxicity and target drug delivery," *Nanomedicine*, vol. 11, no. 1, pp. 81–100, 2016.
[109] Pyroscience, "FireStingO 2 Fiber-Optic Oxygen Meter - The future in oxygen sensing with proven REDFLASH technology," 2018.
[110] J. M. Bolivar, T. Consolati, T. Mayr, and B. Nidetzky, "Shine a light on immobilized enzymes: real-time sensing in solid supported biocatalysts," *Trends Biotechnol.*, vol. 31, no. 3, pp. 194–203, Mar. 2013.

Matlab Algorithm

```
1.
2.  clear
3.  clc
4.  close all
5.
6.  [data,text,raw]=xlsread('green_channel3and4_day2_preNP');% Load Excell file
7.  %%%%%%%%%R%E%Z%A%%%%%%A%F%K%H%M%I%%%%%%%%%%%%%%%%%%%%
    %%%%%%%%%%%%%%%%%
8.  %Stop Flow 1
9.  x_s1=strcmpi(text(:,4),'stop1'); %the comment that we are looking for
10. c_s1=find(x_s1==1);
11. d1_s1=c_s1-4; %row number in data
12. d2_s1=d1_s1+180; %row after 180 seconds
13.
14. %Channel 1
15. ch1v1_s1=data(d1_s1,4); %channel 1 value 1
16. ch1v2_s1=data(d2_s1,4); %channel 1 value 2 ,e.g. after 2min
17. D1_s1=ch1v1_s1-ch1v2_s1; %Delta
18. S1_s1=std(data(d1_s1:d2_s1,4)); %Standard deviation
19. M1_s1=mean(data(d1_s1:d2_s1,4)); %Mean
20. figure
21. plot(data(d1_s1:d2_s1,4),'LineWidth',2)
22. title('Stop Flow 1')
23. hold on
24.
25.
26. %Channel 2
27. ch2v1_s1=data(d1_s1,5);
28. ch2v2_s1=data(d2_s1,5);
29. D2_s1=ch2v1_s1-ch2v2_s1; %Delta
30. S2_s1=std(data(d1_s1:d2_s1,5)); %Standard deviation
31. M2_s1=mean(data(d1_s1:d2_s1,5)); %Mean
32. plot(data(d1_s1:d2_s1,5),'LineWidth',2)
33.
34.
35.
36. %Channel 3
37. ch3v1_s1=data(d1_s1,6);
38. ch3v2_s1=data(d2_s1,6);
39. D3_s1=ch3v1_s1-ch3v2_s1; %Delta
40. S3_s1=std(data(d1_s1:d2_s1,6)); %Standard deviation
41. M3_s1=mean(data(d1_s1:d2_s1,6)); %Mean
42. plot(data(d1_s1:d2_s1,6),'LineWidth',2)
43.
44.
45.
46. %Channel 4
47. ch4v1_s1=data(d1_s1,7);
48. ch4v2_s1=data(d2_s1,7);
49. D4_s1=ch4v1_s1-ch4v2_s1; %Delta
50. S4_s1=std(data(d1_s1:d2_s1,7)); %Standard deviation
51. M4_s1=mean(data(d1_s1:d2_s1,7)); %Mean
52. plot(data(d1_s1:d2_s1,7),'LineWidth',2);
```

```
legend('Channel_1','Channel_2','Channel_3','Channel_4')
xlabel('Time(s)')
ylabel('ppO2')

%Table
Channels = {'Channel_1';'Channel_2';'Channel_3';'Channel_4'};
Delta = [D1_s1;D2_s1;D3_s1;D4_s1];
Standard_deviation = [S1_s1;S2_s1;S3_s1;S4_s1];
Mean = [M1_s1;M2_s1;M3_s1;M4_s1];

T_s1 = table(Delta,Standard_deviation,Mean,...
'RowNames',Channels);
writetable(T_s1,'Stop Flow 1.txt','WriteRowNames',true)

b_s1=[ch1v1_s1 ch1v2_s1; ch2v1_s1 ch2v2_s1; ch3v1_s1 ch3v2_s1; ch4v1_s1 ch4v2_s1];
figure
bar(b_s1)
title('Stop Flow 1')
xlabel('Channel')
ylabel('ppO2')
%%%%%%%%%%%%%%%%%%%%%%%%%%%%%%%%%%%%%%%%%%%%%%%%%%%%%%%%%%%%%%%%%%%%%%%%%%%%%%%%%%%%%%%%%%%%%%%%%%%%%%%%%%%%%%%%%%%%%%%%%%%%%%%%%
%Stop Flow 2
x_s2=strcmpi(text(:,4),'stop2'); %the comment that we are looking for
c_s2=find(x_s2==1);
d1_s2=c_s2-4; %row number in data
d2_s2=d1_s2+180; %row after 180 seconds

%Channel 1
ch1v1_s2=data(d1_s2,4); %channel 1 value 1
ch1v2_s2=data(d2_s2,4); %channel 1 value 2 ,e.g. after 2min
D1_s2=ch1v1_s2-ch1v2_s2; %Delta
S1_s2=std(data(d1_s2:d2_s2,4)); %Standard deviation
M1_s2=mean(data(d1_s2:d2_s2,4)); %Mean
figure
plot(data(d1_s2:d2_s2,4),'LineWidth',2)
title('Stop Flow 2')
hold on


%Channel 2
ch2v1_s2=data(d1_s2,5);
ch2v2_s2=data(d2_s2,5);
D2_s2=ch2v1_s2-ch2v2_s2; %Delta
S2_s2=std(data(d1_s2:d2_s2,5)); %Standard deviation
M2_s2=mean(data(d1_s2:d2_s2,5)); %Mean
plot(data(d1_s2:d2_s2,5),'LineWidth',2)


%Channel 3
ch3v1_s2=data(d1_s2,6);
ch3v2_s2=data(d2_s2,6);
D3_s2=ch3v1_s2-ch3v2_s2; %Delta
S3_s2=std(data(d1_s2:d2_s2,6)); %Standard deviation
M3_s2=mean(data(d1_s2:d2_s2,6)); %Mean
```

```
plot(data(d1_s2:d2_s2,6),'LineWidth',2)



%Channel 4
ch4v1_s2=data(d1_s2,7);
ch4v2_s2=data(d2_s2,7);
D4_s2=ch4v1_s2-ch4v2_s2; %Delta
S4_s2=std(data(d1_s2:d2_s2,7)); %Standard deviation
M4_s2=mean(data(d1_s2:d2_s2,7)); %Mean
plot(data(d1_s2:d2_s2,7),'LineWidth',2);
legend('Channel_1','Channel_2','Channel_3','Channel_4')
xlabel('Time(s)')
ylabel('ppO2')

%Table
Channels = {'Channel_1';'Channel_2';'Channel_3';'Channel_4'};
Delta = [D1_s2;D2_s2;D3_s2;D4_s2];
Standard_deviation = [S1_s2;S2_s2;S3_s2;S4_s2];
Mean = [M1_s2;M2_s2;M3_s2;M4_s2];

T_s2 = table(Delta,Standard_deviation,Mean,...
'RowNames',Channels);
writetable(T_s2,'Stop Flow 2.txt','WriteRowNames',true)

b_s2=[ch1v1_s2 ch1v2_s2; ch2v1_s2 ch2v2_s2; ch3v1_s2 ch3v2_s2; ch4v1_s2 ch4v2_s2];
figure
bar(b_s2)
title('Stop Flow 2')
xlabel('Channel')
ylabel('ppO2')
%%%%%%%%%%%%%%%%%%%%%%%%%%%%%%%%%%%%%%%%%%%%%%%%%%%%%%%%%%%%%%%%%%%%%%%%%%%%%%%%%
%Stop Flow 3
x_s3=strcmpi(text(:,4),'stop3'); %the comment that we are looking for
c_s3=find(x_s3==1);
d1_s3=c_s3-4; %row number in data
d2_s3=d1_s3+180; %row after 180 seconds

%Channel 1
ch1v1_s3=data(d1_s3,4); %channel 1 value 1
ch1v2_s3=data(d2_s3,4); %channel 1 value 2 ,e.g. after 2min
D1_s3=ch1v1_s3-ch1v2_s3; %Delta
S1_s3=std(data(d1_s3:d2_s3,4)); %Standard deviation
M1_s3=mean(data(d1_s3:d2_s3,4)); %Mean
figure
plot(data(d1_s3:d2_s3,4),'LineWidth',2)
title('Stop Flow 3')
hold on


%Channel 2
ch2v1_s3=data(d1_s3,5);
ch2v2_s3=data(d2_s3,5);
D2_s3=ch2v1_s3-ch2v2_s3; %Delta
S2_s3=std(data(d1_s3:d2_s3,5)); %Standard deviation
```

```
M2_s3=mean(data(d1_s3:d2_s3,5)); %Mean
plot(data(d1_s3:d2_s3,5),'LineWidth',2)


%Channel 3
ch3v1_s3=data(d1_s3,6);
ch3v2_s3=data(d2_s3,6);
D3_s3=ch3v1_s3-ch3v2_s3; %Delta
S3_s3=std(data(d1_s3:d2_s3,6)); %Standard deviation
M3_s3=mean(data(d1_s3:d2_s3,6)); %Mean
plot(data(d1_s3:d2_s3,6),'LineWidth',2)


%Channel 4
ch4v1_s3=data(d1_s3,7);
ch4v2_s3=data(d2_s3,7);
D4_s3=ch4v1_s3-ch4v2_s3; %Delta
S4_s3=std(data(d1_s3:d2_s3,7)); %Standard deviation
M4_s3=mean(data(d1_s3:d2_s3,7)); %Mean
plot(data(d1_s3:d2_s3,7),'LineWidth',2);
legend('Channel_1','Channel_2','Channel_3','Channel_4')
xlabel('Time(s)')
ylabel('ppO2')

%Table
Channels = {'Channel_1';'Channel_2';'Channel_3';'Channel_4'};
Delta = [D1_s3;D2_s3;D3_s3;D4_s3];
Standard_deviation = [S1_s3;S2_s3;S3_s3;S4_s3];
Mean = [M1_s3;M2_s3;M3_s3;M4_s3];

T_s3 = table(Delta,Standard_deviation,Mean,...
'RowNames',Channels);
writetable(T_s3,'Stop Flow 3.txt','WriteRowNames',true)

b_s3=[ch1v1_s3 ch1v2_s3; ch2v1_s3 ch2v2_s3; ch3v1_s3 ch3v2_s3; ch4v1_s3 ch4v2_s3];
figure
bar(b_s3)
title('Stop Flow 3')
xlabel('Channel')
ylabel('ppO2')
%%%%%%%%%%%%%%%%%%%%%%%%%%%%%%%%%%%%
%Delta Mean
ch1_D=[D1_s1 D1_s2 D1_s3];
ch1_MD=mean(ch1_D);
ch2_D=[D2_s1 D2_s2 D2_s3];
ch2_MD=mean(ch2_D);
ch3_D=[D3_s1 D3_s2 D3_s3];
ch3_MD=mean(ch3_D);
ch4_D=[D4_s1 D4_s2 D4_s3];
ch4_MD=mean(ch4_D);
%%%%%%%%%%%%%%%%%%%%%%%%%%%%%%%%%%%%%%%%%%%%%%%%%%%%%%%%%%%%%%%%%%%%%%%%%%%%%%%
Channels = {'Channel_1';'Channel_2';'Channel_3';'Channel_4'};
Stop1_Delta = [D1_s1;D2_s1;D3_s1;D4_s1];
Stop2_Delta = [D1_s2;D2_s2;D3_s2;D4_s2];
```

```
Stop3_Delta = [D1_s3;D2_s3;D3_s3;D4_s3];
Mean_Delta=[ch1_MD;ch2_MD;ch3_MD;ch4_MD];

Stop1_Standard_deviation = [S1_s1;S2_s1;S3_s1;S4_s1];
Stop2_Standard_deviation = [S1_s2;S2_s2;S3_s2;S4_s2];
Stop3_Standard_deviation = [S1_s3;S2_s3;S3_s3;S4_s3];

Stop1_Mean = [M1_s1;M2_s1;M3_s1;M4_s1];
Stop2_Mean = [M1_s2;M2_s2;M3_s2;M4_s2];
Stop3_Mean = [M1_s3;M2_s3;M3_s3;M4_s3];

T =
    table(Stop1_Delta,Stop2_Delta,Stop3_Delta,Mean_Delta,Stop1_Standard_deviation,Stop2_Standard_
    deviation,...
Stop3_Standard_deviation,Stop1_Mean,Stop2_Mean,Stop3_Mean,'RowNames',Channels);
writetable(T,'Stop_Flow_Results.xlsx','WriteRowNames',true)
```